Universiteit Utrecht

PRINCETON UNIVERSITY

Department of Earth Sciences

Department of Civil and Environmental Engineering

An investigation of trapping of non-wetting phase during imbibition using pore-network modeling

Master's thesis

Author:
Stan van den Bosch

Supervisors:
S.M. Hassanizadeh
V. Joekar-Niasar
M.A. Celia
F. Doster

August 20, 2012

Contents

1 Abstract

Flow of two phases in porous media plays an important role in for example carbon storage, oil recovery, industrial processes and groundwater contamination problems. The creation of an immobile region of one phase which is completely surrounded by the other phase is referred to as trapping. Pore-network modeling is a useful tool for analyzing two-phase flow and trapping because it is cheap compared to experiments and solving the Navier-Stokes equation on a pore scale. A post-processor which analyzes the results from an existing pore-network model was developed. The pore-network model uses a dynamic two-pressure approach to simulate main imbibition in a regular lattice network of dimensions 10x10x30. The post-processor CSDA (Connectivity and Spatial Distributions Algorithm) locates three phases. These are the wetting phase, connected non-wetting phase and disconnected regions of non-wetting phase within the wetting phase. After that, CSDA calculates properties such as volumes, pressure and shape of disconnected regions and the (spatial distribution of) saturation and pressure of the three phases. These statistics are used to assess the influence of the flow rate, the non-wetting phase viscosity, the variance in pore size and the size of pore throat radii on the dynamics of the trapping of non-wetting phase during imbibition. Trapping can occur due to the snap-off of a single pore, or due to bypassing of the non-wetting fluid by the wetting fluid. If the second mechanism is important, the disconnected regions tend to extend over more pore bodies than if the first mechanism is important. In contrast to what was expected from literature, lower flow rates led to lower trapping. This is attributed to the wetting front becoming sharper, and the wetting films becoming smaller. Increased non-wetting phase viscosity led to lower flow rates. At a similar flow rate, increased non-wetting phase viscosity led to a higher number of disconnected regions and a higher residual saturation. Also, trapping tended to occur in pore bodies with bigger radii. Decreasing the variance in pore body radius led to a lower pore volume. This led to a higher wetting front velocity. The variance in volume of disconnected regions also decreased. This means that the volume of disconnected regions depends on the pore body size. Increasing the pore throat radius led to a higher wetting front velocity since the conductivity of the pore throats went up. This led to a more fingered front. Consequently, trapping due to bypassing was important and the disconnected regions extended over more pore bodies. On the other hand, the increased pore throat radius led to a lower probability of snap-off. This decreased the total number of disconnected regions. So trapping due to snap-off of a single pore was less important and trapping due to bypassing was more important for this scenario.

2 Nomenclature

Some properties can be defined on both a pore-scale and an average scale. Generally, small case letters are used for pore-scale properties (e.g. s for saturation within a pore body), and capital letters are used for domain-average or slice-average properties (e.g. S for saturation in the domain).

Symbol	Meaning	Dimensions
A	Interfacial area	$[L^2]$
Asp	Aspect ratio	[-]
El	Elongatedness	[-]
g	Gravitational accelaration	$[LT^{-2}]$
$\mathbf{K}^{\alpha}$	Effective permeability tensor of phase α	$[L^2]$
K_{ij}^{α}	Conductivity of pore throat ij to phase α	$[L^5T^{-1}F^{-1}]$
$\mathbf{K}_{in}$	Intrinsic permeability tensor	$[L^2]$
K_r^{α}	Relative permeability coefficient of phase α	[-]
L	Length of disconnected region	$[L]$
l_{ij}	Length of pore throat ij	$[L]$
n	Designates non-wetting phase	
$N^{n,dis}$	Number of pore bodies containing disconnected non-wetting phase	[-]
n, dis	Designates disconnected non-wetting phase	
n, con	Designates connected non-wetting phase	
P	Pressure, averaged	$[FL^{-2}]$
p_i^c	Capillary pressure in pore i	$[FL^{-2}]$
p_i^n	Non-wetting phase pressure in pore i	$[FL^{-2}]$
p_i^w	Wetting phase pressure in pore i	$[FL^{-2}]$
$\mathbf{q}^{\alpha}$	Flow rate of phase α	$[LT^{-1}]$
r^*	Mean radius of curvature	$[L]$
r_1, r_2	Radii of curvature	$[L]$
R_i	Radius of inscribed sphere in pore body i	$[L]$
r_{ij}	Radius of pore throat ij	$[L]$
S	Saturation, averaged	[-]
s_i	Saturation in pore body i	[-]
v_i	Volume in pore body i	$[L^3]$
w	Designates wetting phase	
W_1, W_2	Widths of disconnected region	[L]
β	Resistance factor	[-]
θ	Contact angle	[angle]
μ	Viscosity	$[FL^{-2}T]$
ρ	Density	$[ML^{-3}]$
$\sigma^{\alpha\beta}$	Interfacial tension between phase α and phase β	$[FL^{-1}]$
$\Psi^{\alpha a}$	Material property	$[F]$
$\Psi^{\alpha S}$	Material property	$[FL^{-2}]$

3 Introduction

Two-phase flow plays an important role in many porous media, both natural and industrial. Examples include carbon storage in deep geological formations, oil and gas recovery, groundwater contamination problems, soil sciences and numerous industrial processes. The fluid which is preferentially located along the solid matrix of the porous medium is called the wetting fluid and is indicated with the letter w. The fluid which is not preferentially located along the solid matrix is called the non-wetting fluid and is indicated with the letter n. The process of a wetting fluid displacing a non-wetting fluid is referred to as imbibition. In two-phase flow, it is possible that a 'blob' of one phase becomes entirely surrounded by the other fluid. In this case, this blob is referred to as a 'disconnected region', which may extend over multiple pores. Since such a disconnected region is generally assumed to be immobile, the creation of a disconnected region is also referred to as trapping. Trapping in carbon storage is considered desirable since it will prevent the carbon from escaping. The trapping of liquid contaminants will influence their mobility, which can be desirable or not depending on the situation. Trapping in oil recovery is to be avoided since it will lower the total production of oil. Common values of residual oil saturation, which is the fraction of the pore volume which is occupied by the non-wetting phase after the wetting front has passed, are 0.1-0.2 [12] and 0.05-0.4 [15]. This research focuses on the trapping of the non-wetting phase. We wish to find out what effect certain parameters have on the trapping behavior. The research questions are:

- How does trapping happen?
- What is the influence of flow rate on trapping?
- What is the influence of non-wetting phase viscosity, variance in pore size and pore throat radius on trapping?

The influence of flow rate on trapping is a studied separately from the other parameters, because the flow rate may change when changing the last three parameters.
Experiments are expensive and time-consuming to do. Solving the Navier-Stokes equation on a reasonable scale requires too much computational effort. Using pore-network models, one can create virtual porous media to simulate two-phase flow. The advantages of this are that all the parameters can be precisely controlled, there are no measurement issues and it is cheap and quick compared to the other two methods. Therefore, the pore-network model proposed by [13] is used to answer the research questions. The model is run for different scenarios to assess the different parameters. A post-processor is developed to analyze the results. For this research, we only focus on trapping of the non-wetting phase during imbibition.

4 Two-phase flow theory

4.1 Darcy's Law

For experiments with single phase flow in a homogeneous porous medium, [5] found that there was a linear relationship between pressure difference and flow velocity. In this case, the flow rate is given by [1]:

$$\mathbf{q} = -\frac{\mathbf{K}_{in}}{\mu}(\nabla P - \rho \mathbf{g}), \tag{1}$$

where $\mathbf{q}$ is the flow rate $[LT^{-1}]$, $\mathbf{K}_{in}$ is the intrinsic permeability tensor $[L^2]$, μ is the viscosity $[FL^{-2}T]$, P is the pressure $[FL^{-2}]$, ρ is the density of the fluid $[ML^{-3}]$ and g is the gravitational acceleration $[LT^{-2}]$. This equation however, can only be used to describe single phase flow. To describe two-phase flow, an extended form of this equation can be used.

4.2 Extended Darcy's Law

Darcy's law has been generalized for two-phase flow using relative permeabilities. It is commonly assumed that each of the two phases forms its own tortuous paths, which form very stable channels. It is also assumed that for every degree of saturation, there is a unique set of channels [1]. As the phase saturation decreases, there will be less channels available to that phase so the relative permeability of the phase will decrease. We can then use Darcy's law for each phase separately by the introduction of a relative permeability term. The flow of a phase α can be described as follows:

$$\mathbf{q}^\alpha = -\frac{\mathbf{K}_{in}K_r^\alpha}{\mu^\alpha}(\nabla P^\alpha - \rho^\alpha \mathbf{g}), \tag{2}$$

where K_r^α is the relative permeability coefficient of phase α. $\mathbf{K}_{in}K_r^\alpha$ can also be written as the effective permeability tensor $\mathbf{K}^\alpha$. It has been found however, that the pressure difference is not the only driving force. Therefore, a saturation and interfacial area term have been added to the equation [9], [10].

$$\mathbf{q}^\alpha = -\frac{\mathbf{K}^\alpha}{\mu^\alpha}(\nabla P^\alpha - \rho^\alpha \mathbf{g} - \Psi^{\alpha a}\nabla a^{nw} - \Psi^{\alpha S}\nabla S^\alpha) \tag{3}$$

Where $\Psi^{\alpha a}$ is a material property $[FL^{-1}]$, a^{nw} is the specific area of fluid-fluid interfaces $[L^{-1}]$ (amount of interfacial area per unit volume of the porous medium), $\Psi^{\alpha S}$ is a material property $[FL^{-2}]$, and S^a is the saturation.

4.3 Capillary Flow

In this section, we will describe the movement of fluids due to capillary forces. The explanations are largely taken from [1]. When a liquid is in contact with another substance, be it another liquid which does not mix with the first, a gas or a solid, there is a free interfacial energy present between them. This interfacial energy is due to the difference between the inward attraction of the molecules in the interior of each phase and those at the surface of contact. Since a surface possessing free energy contracts if it can do so, the free interfacial energy between phase α and phase β manifests itself as the interfacial tension $\sigma^{\alpha\beta}$ $[FL^{-1}]$. If two immiscible fluids are in contact with a solid at equilibrium, force balance requires the fluid-fluid interface to be at a certain contact angle θ with the solid. By convention, this θ $(0 < \theta < 180^\circ)$ is measured through the denser fluid. When $\theta < 90^\circ$, the fluid is said to be wet to the solid and is called the wetting fluid and is indicated with the letter w. When $\theta > 90^\circ$, the fluid is called a non-wetting fluid and is indicated with the letter n. For the simulations in this work, water is the wetting fluid and air is the non-wetting fluid with $\theta = 0^\circ$. When two immiscible fluids are in contact in the interstices of a

porous medium, a discontinuity in pressure exists across the interface separating them. The difference in pressure is called the capillary pressure:

$$p^c = p^n - p^w, \tag{4}$$

where p^n is the pressure of the non-wetting phase, and p^w is the pressure of the wetting phase. Its magnitude depends on the interface curvature at the point. Here, point refers to the microscopic point inside the void space. The same equation can be used on a Darcy scale:

$$P^c = P^n - P^w. \tag{5}$$

On a pore scale, the local interface curvature is defined by two principal radii of curvature, r_1 and r_2, in two orthogonal planes. By considering the change in direction of the forces acting on opposite sides, the following equation is obtained:

$$p^c = \sigma^{nw}\left(\frac{1}{r_1} + \frac{1}{r_2}\right) = \frac{2\sigma^{nw}}{r^*}, \tag{6}$$

where σ^{nw} is the interfacial tension between the non-wetting and the wetting phase $[FL^{-1}]$, r^* is the mean radius of curvature defined by the harmonic mean of the two principal radii of curvature. Equation 6 is known as the Laplace equation for capillary pressure. The mean radius of curvature is in the order of the pore size. Note that p^c refers to the capillary pressure on a microscopic or pore-scale, and P^c refers to the macroscopic pressure difference between the two fluids. There are various ways of determining P^c, which will not be discussed in this work. The case where a porous medium is initially saturated with a wetting fluid and a non-wetting fluid invades the medium is called drainage. The process where a wetting fluid invades a medium initially saturated with non-wetting fluid is called imbibition. If a sample is completely saturated with a non-wetting fluid, and some wetting fluid is introduced on its surface, the wetting fluid will tend to flow in spontaneously along the solid walls of the pores, displacing the non-wetting fluid. In a vertical displacement, equilibrium is reached when the wetting fluid has accumulated in those pores that permit the greatest curvatures of the fluid-fluid interfaces, i.e. in the smallest pores.

4.4 Displacement mechanisms

In [15], the authors distinguish two distinct displacement mechanisms. Trapping can occur due to both mechanisms. The first is piston-like advance where the displacing fluid advances in a connected front that occupies the center of the pore space. The displacing fluid always resides behind the front. In imbibition, a second type of displacement is distinguished which is due to flow in the corners and crevices of the porous medium. Through these features, the wetting fluid can maintain hydraulic continuity and conductance. This means that pore bodies and pore throats can fill ahead of the connected front. This type of flow is referred to as film flow or corner flow. In [19], the authors state that flow in thin liquid films is likely to become important at low wetting phase saturations.

Characteristics of the wetting front. The wetting front can have different characteristics. It can be sharp, in which case the front will have a planar shape. The front can also be more irregular. Viscous fingering is a macroscopic instability of the wetting front, which occurs for imbibition when the non-wetting phase viscosity exceeds that of the wetting phase [20]. When viscous fingering occurs during imbibition, fingers of wetting phase develop which extend beyond the rest of the wetting front. This can occur at any length scale. Fingering whose characteristic length scale ranges from one to a few pores has been called microfingering and occurs for any viscosity ratio.

4.5 Trapping mechanisms

In two-phase flow in porous media, trapping is the creation of a region of one phase which is completely surrounded by the other phase. Such a region is thus disconnected from the rest of that phase. The

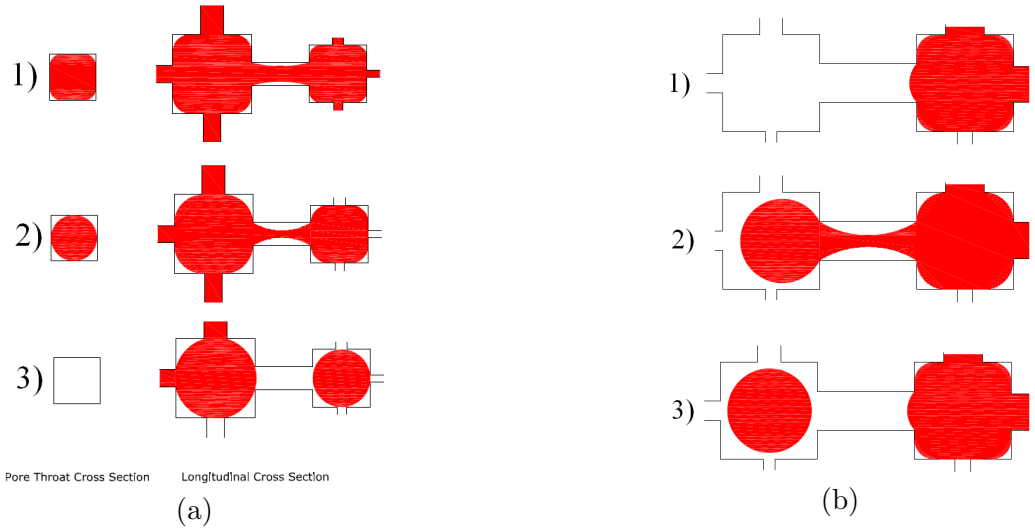

Figure 1: Schematic representation of occurrence of snap-off during (a) imbibition, and during (b) drainage. Red corresponds to the non-wetting phase. Figure from [13].

amount of trapping can be expressed in terms of the residual saturation. The residual saturation is the saturation of the non-wetting phase which cannot be mobilized after the wetting front has passed.

Piston-like movement: trapping due to bypassing. For piston-like movement, trapping can occur when the invading fluid flows around the receding fluid. Since the pores are interconnected and pore sizes are distributed randomly, fluid will flow faster in some pores than in others. Consequently, a portion of the displaced phase can become entirely surrounded by the injected phase [15]. This kind of trapping is referred to as trapping by bypassing and is more important if the wetting front is more irregular.

Corner and film flow: trapping due to snap-off. As the wetting phase liquid films in the corner of the pore throats swell, it is possible that the wetting phase eventually blocks the pore throat (Figure 1a). This phenomenon is referred to as snap-off and was first described in [17] and [18]. According [3], entrapment due to snap-off may account for up to 80% of the residual non-wetting phase.

Snap-off during drainage. Snap-off can also occur during drainage (figure 1b). But since snap-off is related to the ability of the wetting phase to choke off the non-wetting phase, it is more important during imbibition than during drainage [13]. In Figure 1b, we see how snap-off occurs during drainage. As the pressure in the right pore body builds up, it will eventually invade the adjacent pore throat and flow into the next pore body. If it can not entirely fill the next pore body, it will become disconnected again. This process continues intermittently until the non-wetting phase in both pore bodies can stay connected without snap-off.

The effect of flow rate on trapping. The flow rate is often expressed as the capillary number, which is defined for imbibition as:

$$Ca = \left(\frac{\mu_w q_w}{\sigma^{nw}}\right). \tag{7}$$

The significance of capillary number on trapping has been shown in [2, 4, 6–8, 11, 14–16, 20]. A high flow rate inhibits the formation of a arc meniscus in the pore throat which chokes of the non-wetting phase. So snap-off occurs less frequently for high flow rates. Also, when viscous forces are important compared to capillary forces, it is easier for the non-wetting phase to invade a pore throat containing only

wetting phase. Disconnected regions are therefore more likely to be mobile. Since viscous forces tend to fragment disconnected regions, the number of disconnected regions goes up but the volume of individual disconnected regions go down for high flow rates.

The effect of non-wetting phase viscosity on trapping. Previous experiments and modeling efforts have shown that trapping increases for low viscosity ratios [2,4,6,7,11,15,20]. The viscosity ratio M for imbibition is defined as

$$M = \frac{\mu^w}{\mu^n}, \tag{8}$$

where M is the viscosity ratio for imbibition. The case where $M < 1$ holds the viscosity ratio is called unfavorable, and when $M > 1$ holds, the viscosity ratio is called favorable. Viscous fingering occurs more for low M values, especially when the viscosity ratio is unfavorable. If the resistance to flow of the non-wetting phase increases, the wetting phase will tend to flow more around the non-wetting phase. This increases the amount of trapping due to bypassing and due to snap-off, so it is expected that trapping increases when the non-wetting phase viscosity is increased.

The effect of variance in pore body size on trapping. Investigating the effect of variance in pore body size can shed light on the question whether or not there is a pore body size for which trapping preferentially occurs.

The effect of pore throat radius on trapping. The influence of the pore throat radius on trapping has been studied in numerous works [6,7,15,20]. Generally, the pore throat radius is measured relative to the pore body size. This is called aspect ratio and is defined as

$$Asp = \frac{R_i}{r_{ij}}, \tag{9}$$

where R_i is the radius of an inscribed sphere in the pore body i $[L]$ (so the cube side length is $2R_i$), and r_{ij} is the radius of the pore throat between pore bodies i and j. The radius of a pore throat is defined as half the width of the pore throat. A high aspect ratio has two effects [15]. First, it decreases the volume needed to form a stable arc meniscus in the pore throat in comparison to the volume needed to fill the upstream pore body. Second, corner flow is more important for high aspect ratios at low capillary numbers. Both factors reduce the time needed for snap-off to happen and therefore favor pore throat filling ahead of the front. So, increasing the pore throat radius is expected to decrease the amount of trapping.

The effect of network structure on trapping. The coordination number is the number of connections a pore body has with other pore bodies. A low coordination number leads to more trapping, because the number of escape paths of the non-wetting phase is reduced [15]. In [15], it is stated that pore sizes with a random, uncorrelated distribution are unlikely to be representative of geologic porous medium. If the pore sizes are correlated, the permeability in a pore body will be more similar to its neighbors than if the pore sizes are uncorrelated. Therefore, the front will be more prone to fingering when the pore sizes are correlated. This is expected to lead to an increase of the amount of trapping.

5 The pore-network model

Experiments are time consuming and expensive. Using the Navier-Stokes equations to solve two-phase flow on a macro scale requires too much computational effort. Using pore-network models, one can create virtual porous media to simulate various experiments which is cheaper than the other two options. Therefore, pore-network modeling is used for this research.

5.1 Model features

For this research, a pore-network model is used for simulating imbibition. The dynamic two-pressure pore-network model by [13] is used. Some instructions concerning this model are given in Appendix A. Here, only a brief description of the model is provided. For details, please refer to [13]. The pore-network model consists of pore bodies, which are connected by pore throats. The pore bodies represent the volumetric properties of a porous medium, and are assumed to have no hydraulic resistance. The pore throats on the other hand, are assumed to have no volume and represent the hydraulic resistance of the porous medium. It is thus assumed that filling a pore throat does not take time. The pore bodies have sizes which follow a specifiable probability distribution and are uncorrelated in space. Pore throat sizes are calculated from the pore body sizes. Based on the specified model dimensions, fluid properties, pore size distribution properties, initial conditions and boundary conditions, it generates the pore sizes and calculates the evolution in time of the distribution of the fluids and the pressures. The pore-network model only provides the non-wetting phase pressure p_i^n as an output, so the wetting phase pressure p_i^w is calculated in the post-processor CSDA (Section 6). In the pore bodies where there is no non-wetting phase, the model outputs a representative p_i^n which can be used to calculate p_i^w. When there is no non-wetting phase in a pore body, the capillary pressure is equal to zero. The model uses cubic pore bodies, and pore throats with a square cross section. This means that there is always some wetting phase residing in the corners of pore bodies and pore throats. Corner flow is therefore possible, and the wetting phase is assumed to always be connected to the wetting phase boundary. A pore throat can have two states: either it contains only wetting phase, or it contains both wetting and non-wetting phase. The pore-network model does not allow a pore body to contain only non-wetting phase. For that to happen, an infinite capillary pressure would be required. If a pore throat contains only wetting phase, the conductivities of a pore throat can be calculated by:

$$K_{ij}^w = \frac{\pi}{8\mu^w l_{ij}} (r_{ij}^{w,\text{eff}})^4, \tag{10}$$

$$K_{ij}^n = 0, \tag{11}$$

where K_{ij}^w is the conductivity for the wetting phase of a pore throat ij $[L^5T^{-1}F^{-1}]$, K_{ij}^n is the conductivity for the non-wetting phase of a pore throat ij $[L^5T^{-1}F^{-1}]$, l_{ij} is the length of the pore throat $[L]$, and

$$r_{ij}^{w,\text{eff}} = \sqrt{\frac{4}{\pi}} r_{ij}, \tag{12}$$

is an effective pore throat radius for single phase flow. In case there is both wetting and non-wetting phase in a pore throat, the conductivities are given by

$$K_{ij}^w = \frac{4-\pi}{\beta\mu^w l_{ij}} (r_{ij}^c)^4, \tag{13}$$

$$K_{ij}^n = \frac{\pi}{8\mu^n l_{ij}} (r_{ij}^{n,\text{eff}})^4, \tag{14}$$

where β is a resistance factor that depends on geometry, surface roughness, crevice roundness and other specifications of the cross section [-], and

$$r_{ij}^c = \frac{\sigma^{nw}}{p_{ij}^c}, \tag{15}$$

$$r_{ij}^{n,\text{eff}} = \frac{1}{2}\left(\sqrt{\frac{r_{ij}^2 - (4-\pi)r_{ij}^{c^2}}{\pi}} + r_{ij}\right), \tag{16}$$

where $r_{ij}^{n,\text{eff}}$ is an effective pore throat radius for two-phase flow $[L]$ and the capillary pressure in the pore throat ij, p_{ij}^c is determined by the capillary pressure p_i^c in the upstream pore body i:

$$p_i^c = \begin{cases} \frac{2\sigma}{R_i(1-\exp(-6.83*s_i^w))}, & s_i^w < 0.48, \\ \frac{2\sigma}{R_i(1-\exp(-6.83*0.48))}, & 0.48 \leq s_i^w < 1, \\ 0, & s_i^w = 1, \end{cases} \tag{17}$$

where s_i^w is the saturation of the wetting phase in pore body i. This equation is also used in CSDA to calculate the wetting phase pressure from the non-wetting phase pressure. The structure of the network is lattice, meaning that the pore bodies are positioned at the vertices of a regular lattice. Unless mentioned otherwise, the simulations are done with 10x10x30 pore bodies, with the 30 pore bodies in the direction of flow. This elongated shape was chosen because boundary effects were expected to be strongest at the in and outflow boundaries. The spaces between the layers in the three directions are variable. Each pore body, with the exception of those at the upstream and downstream boundaries, is connected to its six neighbours. At the upstream and downstream boundaries, the domain is conceptually connected to fluid reservoirs, so the pore bodies there are connected to five other pore bodies and to the fluid reservoir. To minimize side boundary effects, a periodic boundary condition is used for the sides which are perpendicular to the flow. This means that fluids which flow out from one boundary, will flow in at the opposite boundary. The fluids are assumed to be incompressible and immiscible. Snap-off in a pore throat ij occurs for:

$$p_{ij}^c \leq \frac{\sigma^{nw}}{r_{ij}}. \tag{18}$$

This is the same snap-off criterion as used in [11].

5.2 Boundary and initial conditions

In this section, we will present the boundary and initial conditions for free imbibition and for controlled imbibition. The domain is connected to a wetting phase reservoir on one side, and to a non-wetting phase reservoir on the other side. We will refer to the wetting phase boundary as the left boundary, and to the non-wetting phase boundary as the right boundary. This means that for imbibition, flow is from left to right.

Free imbibition. Free imbibition refers to the case where there is no imposed pressure gradient in the domain. This means that the pressures in both reservoirs are set to zero. At the wetting phase boundary, there are two layers, located on planes perpendicular to the flow, which are initially completely saturated with wetting phase, i.e. for every pore in those layers $s_i^w = 1$. As in all pore bodies, the wetting phase pressure in the pore bodies closest to the non-wetting phase boundary is given by $p_i^w = p_i^n - p_i^c$, where p_i^c is given by equation (17). The capillary pressure of the pore throats connecting these pore bodies to the non-wetting phase reservoir is equal to the capillary pressure in the pore body which it is connected to. At the wetting phase boundary the permeability of the non-wetting phase is 0. Initially, there is a saturation throughout the domain which, with the exception of the two layers of pore bodies at the wetting phase boundary, corresponds to a specified initial capillary pressure p^c. The initial saturation is calculated using the inverse relation of equation (17). The boundary and initial conditions are represented in Figure 2.

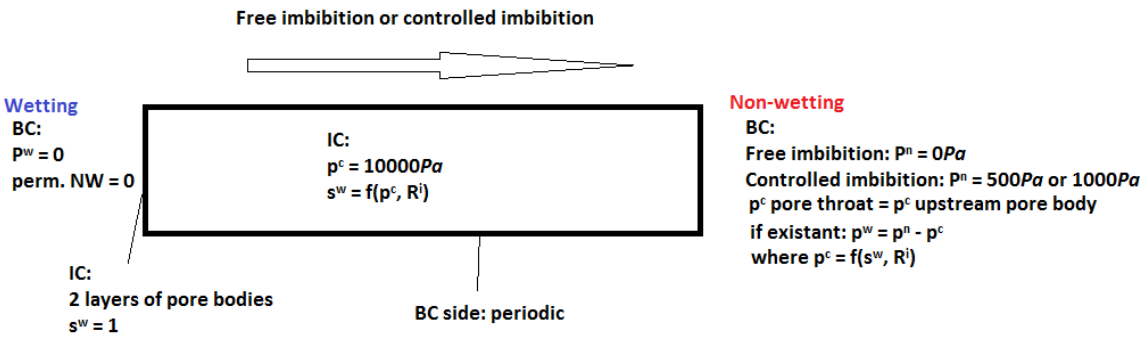

Figure 2: Scheme of boundary and initial conditions of the pore-network model

Controlled imbibition. Controlled imbibition refers to the case where a pressure gradient is imposed which opposes the flow. All the boundary and initial conditions are the same as for free imbibition, except for the non-wetting phase boundary. It is set to either 500Pa or 1000Pa.

6 The post-processor CSDA

In this section, the post-processor which was developed for this research is presented. It is called CSDA (Connectivity and Spatial Distributions Algorithm). It uses output from the pore-network model, and calculates several parameters pertaining mainly to the trapped non-wetting phase (Figure 3). The pseudocode of CSDA is given in Appendix B. An overview of the output files which CSDA generates is provided in Appendix C. An overview of the matlab scripts used for plotting the results is given in Appendix D.

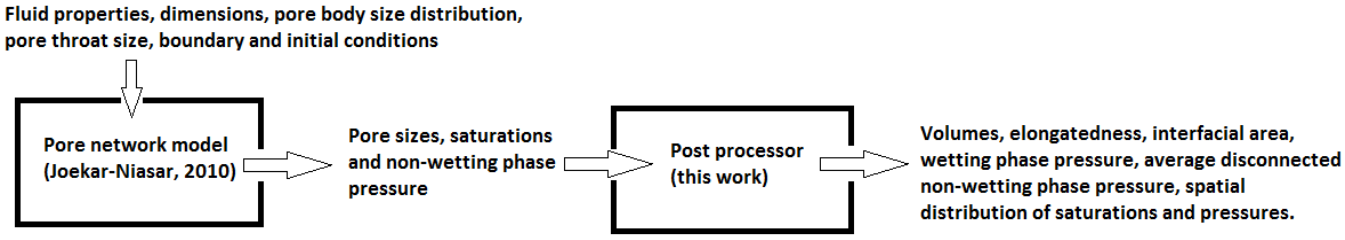

Figure 3: The workflow

6.1 Model features

Here, we will describe the general way CSDA works. It is a code developed in Fortran 95, and Matlab is used to plot the Figures. The most important feature of it is that it distinguishes 'connected' and 'disconnected' non-wetting phase. To do so, the pore bodies connected to the non-wetting phase boundary are given the same unique number. Then, for every other pore body containing non-wetting phase, it is decided to what other pore bodies containing non-wetting phase it is connected. All the pore bodies in this 'cluster' or 'disconnected region' get the same unique number. When we know what non-wetting phase is disconnected and what non-wetting phase is connected, we can calculate spatial averages of for example disconnected non-wetting phase pressure. We can also perform several calculations on the disconnected regions such as calculate its volume, interfacial area or elongatedness.

6.2 Calculation of parameters

Here, we will explain how CSDA's calculations are done.

Volume of a phase. Remember from section 5.1 that pore throats are assumed to have no volume. The volume of a phase α in a pore body i is calculated by multiplication of the phase saturation by the pore body volume:

$$v_i^\alpha = s_i^\alpha (2R_i)^3, \tag{19}$$

where α can be w, n, dis or n, con. The total volume of a phase in the domain is found by summing the volume of that phase in all the pore bodies.

Total pore volume. The total pore volume is calculated by summing the volume of all the pore bodies in the domain.

Saturations in the domain. To determine the saturation in the domain, the total volume in the domain of a phase is divided by the total pore volume.

Volume of a disconnected region. The volume of a disconnected region is determined by adding the volumes of the disconnected non-wetting phase of all the pore bodies within that disconnected region.

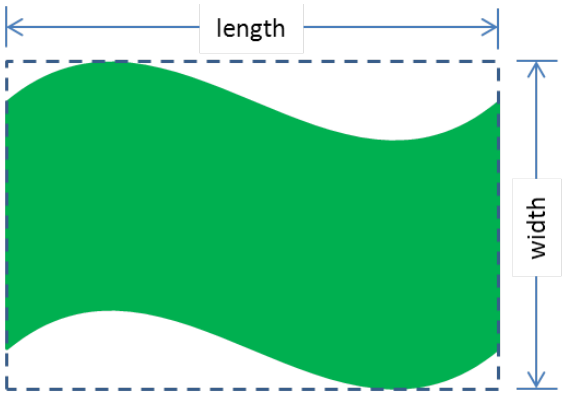

Figure 4: Length and width for the calculation of the elongatedness of a disconnected region in two dimensions. Figure from [22].

Elongatedness. The elongatedness of a disconnected region can be calculated in two dimensions by dividing the length of a disconnected region by its width (Figure 4). The length is defined as the distance in the direction of the flow between the most upstream and the most downstream pore body. The width is defined as the distance perpendicular to the flow between the most far-lying pore bodies. In three dimensions, we can add one more width, which is perpendicular to both the first width and the length:

$$El = \frac{2L}{W_1 + W_2}, \tag{20}$$

where El is the elongatedness [-], L is the length of the disconnected region $[L]$, and W_1 and W_2 are the widths of the disconnected region $[L]$. The length and the widths are determined based on the indices of the pore bodies, so along the planes that define the lattice. A disconnected region which is elongated in the direction of the flow has a value larger than 1. While the spacing in between pore bodies may differ, we have chosen to use the indices of the pore bodies instead of the real distance. This is acceptable because the spacing between the pore bodies does not vary much.

Domain-average disconnected non-wetting phase pressure. For the calculation of average disconnected non-wetting phase pressure, we have chosen to take the arithmetic mean of the pressure values of all the pore bodies containing disconnected non-wetting phase,

$$P^{n,dis} = \frac{1}{N^{n,dis}} \sum_{i=1}^{N^{n,dis}} p_i^n, \tag{21}$$

where $P^{n,dis}$ is the average disconnected non-wetting phase pressure in the domain $[FL^{-2}]$, $N^{n,dis}$ is the number of pore bodies in the domain containing non-wetting phase and p_i^n is the non-wetting phase pressure in pore body i $[FL^{-2}]$.

Wetting phase pressure. The pore-network model outputs the non-wetting phase pressure and the saturation of wetting phase, which can be used to calculate the wetting phase pressure. It is calculated by $p_i^w = p_i^n - p_i^c$, where p_i^c is given by equation (17). Since cubic pore bodies are used, there is always some wetting phase residing in the corners of a pore body. Therefore, there is a p_i^w value for every pore body.

Interfacial area. Interfacial area is denoted by the letter A $[L^{-1}]$. Since the pore throats are assumed to have no volume, there is also no interfacial area in the pore throats. There are two types of

interfaces [13]: corner interfaces and main terminal menisci. Corner interfaces are interfaces in corners and edges of a pore body. Main terminal menisci are interfaces which cover the entrance of a pore throat, in case there is non-wetting phase in the pore body and no non-wetting phase in the pore throat. The total specific interfacial area and the specific interfacial area of the main terminal menisci of pore bodies containing disconnected non-wetting phase are outputs of the pore-network model. However, because we want to learn more about the interfacial area of each individual disconnected region, we have to calculate the interfacial area from the saturation of the wetting phase and the radius of a pore body. From [13], we obtain the following equations:

$$R_{i,eq} = \begin{cases} R_i(\frac{6}{\pi}(1 - s_i^w))^{1/3}, & s_i^w \geq 0.48, \\ R_i(1 - exp(-6.83 s_i^w)), & s_i^w < 0.48, \end{cases} \tag{22}$$

$$A_i^{nw} = \begin{cases} 4\pi R_{i,eq}^2, & s_i^w \geq 0.48, \\ 4\pi R_{i,eq}^2 + 6\pi R_{i,eq}(R_i - R_{i,eq}), & s_i^w < 0.48, \end{cases} \tag{23}$$

where $R_{i,eq}$ is an equivalent radius $[L]$, and A_i^{nw} is the interfacial area of pore body i $[L^2]$ due to corner interfaces. For the interfacial area of a main terminal meniscus, the following equation is used:

$$A_i^{nw} = 8\pi \left(\frac{\sigma^{nw}}{p_i^c}\right)^2 \left(1 - \sqrt{1 - \left(\frac{r_{ij} p_i^c}{2\sigma^{nw}}\right)^2}\right), \tag{24}$$

where A_i^{nw} is the interfacial area of a main terminal meniscus and p_i^c is given by equation (17). Note that when $r_{ij} p_i^c > 2\sigma^{nw}$, a complex number will result. This only occurs when both p_i^c and r_{ij} are high. If the radius of a pore throat is high, the entry capillary pressure is low. It is rare that the capillary pressure in the pore body is high and the pore throat is large, since invasion by the wetting phase will generally have resulted before build-up of capillary pressure. In the rare cases this situation does occur, A_i^{nw} is set to zero. To calculate the interfacial area in a pore body, the interfacial area due to corner interfaces and the interfacial area due to main terminal menisci are summed.

Specific interfacial area. The specific interfacial area of a disconnected region is calculated by dividing its interfacial area by the domain volume. The domain volume includes both pore space and solid matrix. Sometimes, the interfacial area is expressed as the interfacial area of a disconnected region divided by the volume of that disconnected region $\left(\frac{A}{v}\right)$.

Spatial distributions of pressure and saturation. In some cases, we want to look at the spatial variation of pressure or saturation along the column. We divide the domain in 30 10x10 slices which are perpendicular to the flow direction. We can plot the saturation or pressure value for each slice, in which case we call the graph 'unsmoothed'. The saturation value of a slice is determined by calculating the total non-wetting phase volume in a slice, and dividing by the total fluid volume in that slice. The non-wetting phase pressure value of a slice is determined by summing all the non-wetting phase pressure values for pore bodies containing non-wetting phase in that slice, and dividing it by the number of pore bodies containing non-wetting phase in that slice. If there is no non-wetting phase in a slice, a value of 0 is used for both the saturation and the pressure. The wetting phase pressure is calculated by summing all the wetting phase pressure values, and dividing by 100 (the number of pore bodies in a slice). We can also smooth the graph in order to make the graphs more readable and to accentuate the trend in the graph. In this case, the graph is referred to as 'smoothed'. For each slice, we consider also its neighbors for determining the value. For the first and the last slice, this means we consider two slices, and for all the other slices we consider three slices. For saturation, we divide the volume of non-wetting phase in the slices by the total fluid volume in the slices. For pressure, we use the average of the values calculated for the unsmoothed graph. An improvement to this would be using a similar approach as for the smoothed

saturation distribution, since if a slice contains no non-wetting phase, the slice value of 0 will be used in the averaging procedure while one would rather not take it into account at all. However, the smoothed plots of pressure still accomplish their goal, which is to show the spatial variation of pressure.

Number of pore bodies occupied by a disconnected region. Within every disconnected region, this parameter is calculated by summing the number of pore bodies which contain disconnected non-wetting phase.

7 The scenarios

Two research questions for this research are: What is the influence of non-wetting phase viscosity, variance in pore body size and pore throat radius on trapping? What is the influence of flow rate on trapping? In order to answer these questions, 6 different simulations are executed. All scenarios are imbibition simulations for a 10x10x30 pore-network model. The first scenario is a reference scenario and corresponds to a water-air system subject to free imbibition. For the other five scenarios, we change one parameter with respect to the first. The values are chosen such that the effect of changing this parameter is clear in the results. The scenarios are:

1. **Reference:** a free imbibition water-air system
2. **Controlled imbibition 1:** the pressure in the non-wetting phase reservoir is increased from 0Pa to 500Pa. The same realization of the pore size distribution is used as for scenario 1.
3. **Controlled imbibition 2:** the pressure in the non-wetting phase reservoir is increased from 0Pa to 1000Pa. The same realization of the pore size distribution is used as for scenario 1. Increasing the pressure more resulted in incomplete imbibition and model errors.
4. **Increased non-wetting phase viscosity:** the non-wetting phase viscosity μ^n is increased from $1.5 \cdot 10^{-5}$Pa s to $5 \cdot 10^{-4}$Pa s, leading to a viscosity ratio of 2. The same realization of the pore size distribution is used as for scenario 1.
5. **Low variance in pore body size:** the variance in pore body radius is decreased from 0.5mm^2 to 0.3mm^2.
6. **Increased pore throat radius:** the pore throat radius is on average 1.25 bigger. Increasing the pore throat radius more would lead to bigger throats than pore bodies in some places, causing the pore-network model to generate an error.

An overview of the parameters which are used for these scenarios is presented in Table 1.

Variable	Symbol	Value 1) Reference	Value other scenarios	Unit
Number of pores	f	10x10x30; 30 in flow direction		-
Mean pore body size		0.07		mm
Minimum pore body size		0.01		mm
Maximum pore body size		0.2		mm
Contact angle	θ	0		degree
Interfacial tension	σ^{nw}	0.0725		Nm^{-1}
Initial capillary pressure	Initial P^c	10000		Pa
Viscosity of wetting phase	μ^w	0.001		Pa s
Viscosity of non-wetting phase	μ^n	0.000015	Scenario 4): 0.0005	Pa s
Variance pore body size		0.5	Scenario 5): 0.3	mm^2
Pore throat coeff (to make pore throats larger)		1	Scenario 6): 1.25	-
Non-wetting phase boundary pressure		0	Scenario 2): 500, Scenario 3): 1000	Pa

Table 1: The input parameters used for the six scenarios.

8 Results and discussion

8.1 General results

8.1.1 Visualization of spatial fluid distribution

General flow dynamics are studied using results from the reference scenario. This scenario has been run 4 times, and it was found that the results presented here are typical for this scenario. A longitudinal cross section of the wetting phase saturation of the middle of the domain is shown in Figure 5. Every square corresponds to one pore body. Since the model has 10x10x30 pores, this cross-section has 10x30 pores. Blue corresponds to a high wetting phase saturation s_i^w, and red corresponds to a low s_i^w. s_i^w is high on the left, and low on the right. The left part of the domain is the 'wet' part, and the right part is the 'dry' part. Flow is from left to right. The front is located where the blue and red squares are closest. At the front, there are intermediate colors which correspond to an intermediate saturation. Some cells in the wet part also have an intermediate saturation. The front is not entirely straight: in the top three rows the front is located more to the right than for rows 4 - 6. In the dry part the saturation values are not uniform but vary between 0.01 and 0.1. This variation is due to the fact that initially, the capillary pressure is 10000Pa in every pore body. The pore bodies have different radii. For a different pore body radius, there is a different saturation which corresponds to the initial capillary pressure (equation 17).

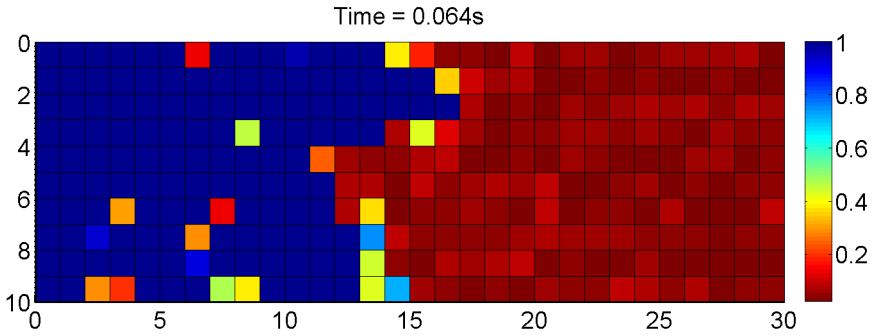

Figure 5: Saturation of wetting phase in a longitudinal cross-section of the middle of the domain. Every square corresponds to a pore body. For the reference 10x10x30 free imbibition scenario (scenario 1).

8.1.2 Spatial distribution of saturation and pressure

Spatial distributions of saturation and pressure for two stages of imbibition are shown in Figure 6. On the left an early stage of imbibition is shown, and on the right an intermediate stage. On the right side of Figures 6a and 6b we observe that $S^w + S^{n,dis} = S^w \approx 0.05$. This value corresponds to the initial saturation of the wetting phase. On the left side of Figure 6b we observe that $(S^w + S^{n,dis}) - S^w = S^{n,dis} \approx 0.05$. This value corresponds to the residual saturation of the non-wetting phase. Compared to $[3, 6, 12, 15, 21]$, this value is low. Possibly, the reasons for this is that most systems which are studied in literature are water-oil systems, whilst the results presented in this research are for a water-air system. Another possible reason is that the coordination number is constant at a value of 6, so the non-wetting phase always has several escape routes. Finally, the pore sizes are uncorrelated for the pore-network model, which leads to a lower amount of fingering and thus trapping than when the pore sizes are correlated (Section 4.5). The transition between the zones where $S^w + S^{n,dis}$ goes from 1 to 0.05 extends over only five pore bodies. This transition zone corresponds to the wetting front. Remember that this figure is smoothed, so in reality the wetting front is smaller. The wetted part of the domain is left of the front, and the dry part of the domain is right of the front. In the dry part of the domain in Figures 6c and 6d, we observe that $P^w = -10000$Pa. This value corresponds to the initial condition. $P^w = 0$ on the left boundary and goes down to the right, which drives the flow from left to right. The steepest slope

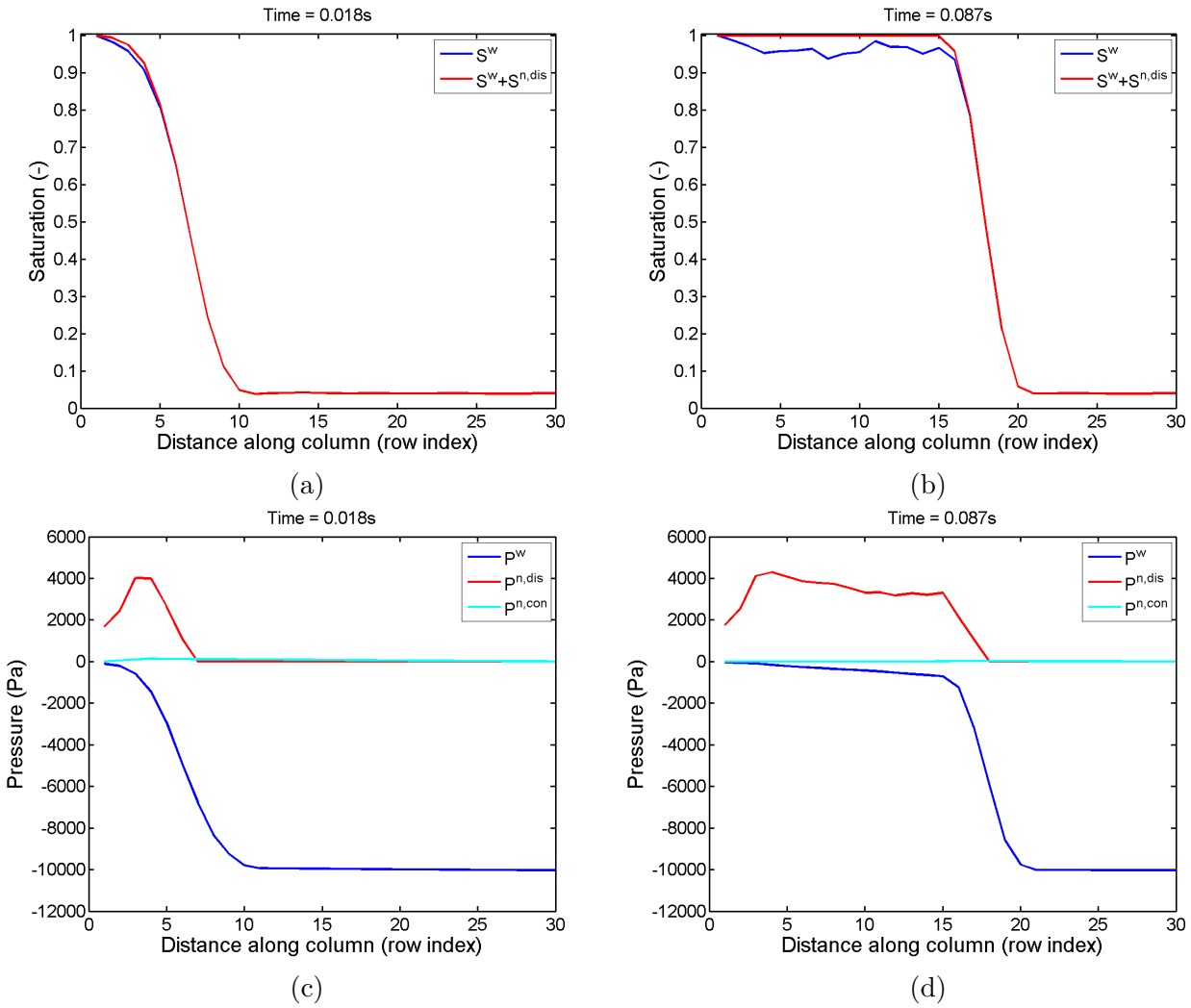

Figure 6: Spatial distributions of (a & b) saturation and (c & d) pressures at two stages of imbibition. For the reference (scenario 1) 10x10x30 free imbibition run.

in S^w is observed at the wetting front. The slope of the connected non-wetting phase pressure $P^{n,con}$ in Figures 6c and 6d is gentle compared to that of the wetting phase pressure P^w. The slope of the disconnected non-wetting phase pressure is comparable to that of the wetting phase pressure. On the left side of Figures 6c and 6d, there seems to be a gradient in P^n towards the wetting phase boundary. However, the low value at the left boundary is due to the fact that a value of 0 is plotted if no values are available. Because the graph is smoothed, it seems that this gradient is present over more than one slice which would mean countercurrent flow, but this is actually not the case. The slope of $P^{n,con}$ is more gentle than the slope of P^w, since although the flow rate is comparable, the mobility of the non-wetting phase is higher due to the lower viscosity of air. Indeed, when increasing the non-wetting phase viscosity (scenario 6), we observe a steeper gradient for $P^{n,con}$ (figure not provided). Although there is a gradient in the disconnected non-wetting phase pressure $P^{n,dis}$, we do not observe flow of the non-wetting phase (figure not provided). Under the incompressibility assumption, this means that the saturation and the shape of the non-wetting phase in the pore body do not change. Thus, the radius of curvature and the capillary pressure p_i^c are constant after disconnection. Not every disconnected region will have the same capillary pressure, but because we are averaging the pressures, it is also more or less constant throughout the wetted part of the domain. Since the non-wetting phase is completely contained within the wetting phase and the P^c of the wetted part of the domain is constant in time, we argue that the gradient in

$P^{n,dis}$ is due to the gradient in P^w. The gradient in P^w is highest near the wetting front since the relative permeability of the wetting phase is low here. This leads to lower conductivity and a higher energy dissipation.

8.1.3 Spatial and temporal pressure distribution

Unsmoothed spatial distributions of the pressures in time are shown in Figure 7. Red colors indicate a high value for P^w, $P^{n,dis}$ or $P^{n,con}$, while blue colors indicate a low value. For each plot, the color scale is adapted to better show the full range of values. Figure 7a shows the P^w values. The top part of the graph corresponds to $t = 0s$, and time progresses when going down. On the right, $P^w = -10000$Pa which is due to the initial condition and corresponds to the dry part of the domain. The width over which these values occur decreases in time which corresponds to the dry part of the domain becoming smaller. On the left, $P^w = 0$Pa which corresponds to the boundary condition. The wetting front is located where intermediate pressure values are found, and forms a line from the upper left corner to the lower right corner. The slope of this line shows the velocity of the wetting front. Initially, the slope is gentle, which means a fast-moving front. The slope gradually becomes steeper, so the wetting front slows down. At $t = 0.18$s, the line reaches its gentlest slope yet, corresponding to the highest velocity found for this simulation. The wetting front reaches the non-wetting phase boundary at the right around this time. After the front has reached this boundary, the pressure values increase throughout the domain. Steady state is reached after $0.2s$. Figure 7b shows the $P^{n,dis}$ values. The upper right triangle shows values of zero. This triangle corresponds to the dry part of the domain: since there is no disconnected non-wetting phase, a value of 0 is shown. The first slice also does not contain any disconnected non-wetting phase at any time, so here also $P^{n,dis}$ is shown to be zero. The initial condition for the first two layers was that for every pore body $s_i^w = 0$. However, the second layer does show a positive value after 0.004s, so there is some non-wetting phase there. Like for P^w, the pressure increases throughout the domain when the front reaches the non-wetting phase boundary. $P^{n,con}$ values are shown in Figures 7c and 7d. These figures are the same, but for Figure 7d, the range of values of the color axis is smaller. Values range from -1300Pa to 2000Pa, although Figure 7c indicates that those values rarely occur. Figure 7d shows that for the first 0.004s, $P^{n,con}$ equals zero everywhere. This corresponds to the first time step, for which the pressure field of the non-wetting phase has not yet been calculated. The lower left part of the domain shows values of zero. There is no connected non-wetting phase here, since this is the wet part of the domain.

The fact that the velocity of the wetting front is high initially but gradually decreases is attributed to the decrease in wetting phase pressure gradient. The wetting phase pressure is fixed on the left boundary, and the wetting phase pressure upstream of the wetting front is due to the initial condition and therefore also constant. So the wetting phase pressure difference between the boundary and the wetting front is constant in time. However, the distance between the boundary and the wetting front increases so the pressure gradient must also decrease. When the wetting front is close to the right boundary, the velocity increases again. We attribute this to an increase of the relative permeability of the wetting phase: as the wetting front encounters the extremity of the domain, there are no pore bodies with a low wetting phase saturation to the right of the wetting front anymore. The increase in wetting phase pressure when the wetting front reaches the non-wetting phase boundary is attributed to the fact that there is no connected non-wetting phase left, so there is no suction anymore. The wetting phase pressure therefore is close to the boundary pressures. $P^{n,dis}$ also goes up close to steady state because, as explained before, it depends on P^w.

Figure 8 shows the average disconnected non-wetting phase pressure in time. The pressure starts at zero, since initially there is not yet any disconnected non-wetting phase. In the early stages of imbibition, the highest pressure values are reached. This is attributed to the fact that the average wetting phase pressure upstream of the wetting front is also highest in the early stages of imbibition (Figure 7a). As explained before, the disconnected non-wetting phase pressure depends on the wetting phase pressure. The wetting phase pressure increases close to steady state, since suction decreases because there is less

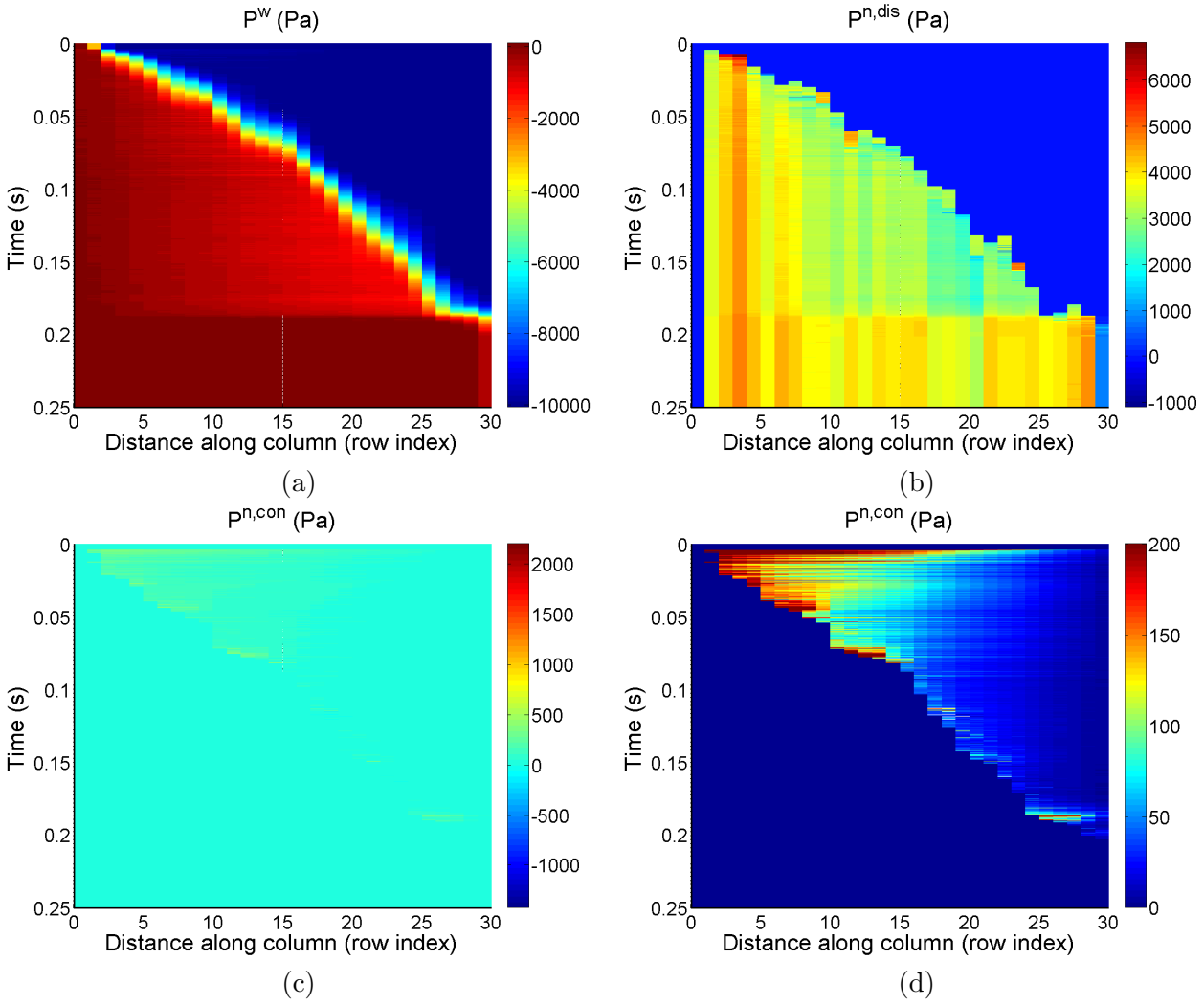

Figure 7: Plots of the unsmoothed spatial distribution (horizontal) in time (vertical) of (a) $P^{n,dis}$,(b) P^{w} and (c)&(d) $P^{n,con}$. For a reference (scenario 1) 10x10x30 free imbibition run.

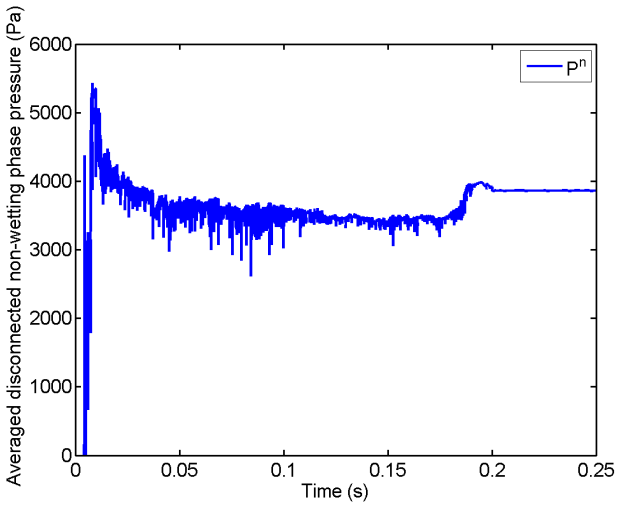

Figure 8: Average disconnected non-wetting phase pressure for the entire domain. For a reference (scenario 1) 10x10x30 free imbibition run.

connected non-wetting phase.

8.1.4 Characteristics of disconnected regions

Figure 9 shows the frequency distribution of the number of pore bodies over which a disconnected region extends. About 90% of the disconnected regions extend over only one pore body.

In view of the fact that most disconnected regions extend over only one pore body, it is expected that the elongatedness is most frequently equal to 1. This is confirmed in Figure 10. Figure 10a shows the elongatedness values for scenario 1 (reference) at $S^w = 0.8$ and Figure 10b shows the elongatedness values for scenario 6 (increased pore throat size) at $S^w = 0.8$. There is more spread in the values of scenario 6 than in the values of scenario 1. In effect, 20% of the values are not equal to one for scenario 6. Values above 1 do not occur more frequently than values below one for either scenario. If the disconnected regions are preferentially elongated in the direction of the flow, values for elongatedness would be greater than one more often than smaller than one. Since this is not the case, we conclude that there is no preferential elongation in the direction of the flow.

The occurrence of disconnected regions with a certain volume is shown in Figure 11. Most disconnected regions have volumes between 0.0001mm^3 and 0.0016mm^3 throughout the model run.

Figure 12 shows the saturation of wetting phase s_i^w and radius of pore bodies containing disconnected non-wetting phase, and the pore size distribution of all the pore bodies. Every dot represents a pore body containing disconnected non-wetting phase, where s_i^w can be read on the y-axis, and R_i can be read on the x-axis. The line corresponds to the pore size distribution of all 3000 pore bodies. If the density of the dots is high in a certain region of the graph, there are many pore bodies containing disconnected non-wetting phase with approximately the s_i^w R_i combination corresponding to that region. Most pore bodies containing disconnected non-wetting phase have radii in the range $0.03\text{mm} < R_i < 0.06\text{mm}$. In this range, the density of the dots is slightly higher for low s_i^w values, but values below $s_i^w = 0.0075$ do not occur. Pore bodies containing disconnected non-wetting phase with a radius between $0.06\text{mm} < R_i < 0.1$ are rare and mostly have a s_i^w value above 0.07. The shape of the pore size distribution corresponds to a truncated lognormal distribution with an average of 0.07mm, a minimum of 0.01mm, a maximum of 0.02mm and a variance of 0.5mm^2 (Table 1). The frequency of occurrence increases sharply at $R_i \approx 0.03\text{mm}$, reaches a maximum at $R_i = 0.04\text{mm}$, then decreases exponentially and goes to zero at $R_i = 0.1\text{mm}$. Values above $R_i = 0.06\text{mm}$ do frequently occur. Even though pore bodies with $R_i > 0.06\text{mm}$ frequently occur, there is little trapping in those pore bodies. So Figure 12 indicates that trapping occurs preferentially in pore

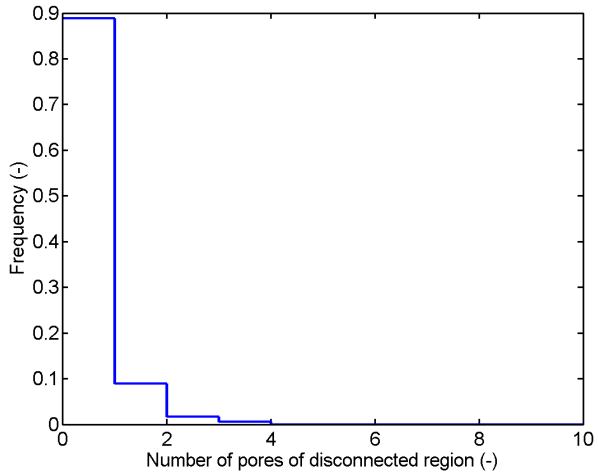

Figure 9: Frequency distribution of the number of pores occupied by a disconnected region for the reference scenario (scenario 1) at $S^w = 0.8$.

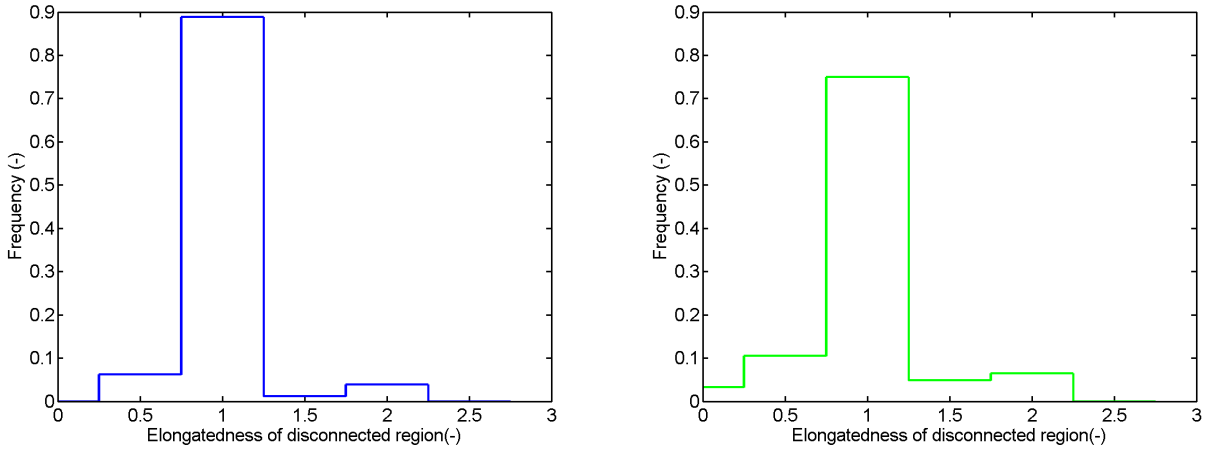

(a) (b)

Figure 10: Frequency distribution of the elongatedness of a disconnected region at $S^w = 0.8$. For (a) the reference (scenario 1) and (b) the increased pore throat size scenario (scenario 6).

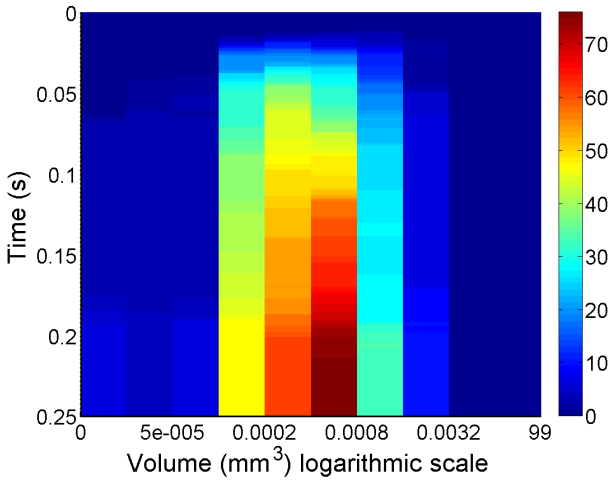

Figure 11: Volume of disconnected regions. Colors correspond to number of occurences within a class. For a reference (scenario 1) 10x10x30 free imbibition run.

bodies with $R_i < 0.06$mm. When trapping does occur in the larger pore bodies, the saturation of wetting phase is generally high.

Figure 13 shows the added specific interfacial area in all pore bodies in blue, and the added specific interfacial area due to main terminal menisci of the disconnected regions in red. We see that initially, the specific interfacial area is highest. This is to be expected since the number of pore bodies containing both wetting and non-wetting phase is also highest. As the number of pore bodies containing both wetting phase and non-wetting phase decreases, so does the total specific interfacial area. Figure 7 showed that as the wetting front reaches the non-wetting phase boundary close to steady state, the velocity of the wetting phase increases. Therefore, most change in the total interfacial area is observed at $t = 0.18$s. Figure 14 shows the frequency distribution of disconnected regions with a certain specific interfacial area at $S^w = 0.8$. The disconnected regions most frequently have a specific interfacial area between 5x10^{-4}mm^{-1} and 2.5x10^{-3}mm^{-1} Figure 15 shows the evolution in time of the interfacial area to volume ratio distribution of the disconnected regions. Throughout the model run, most disconnected region have a ratio between 16mm^{-1} and 64mm^{-1}.

8.2 Evaluation of system size effects

This chapter focuses on the question of whether or not average values of the 10x10x30 domain are meaningful. If they are, our results are useful for improving field-scale models. There are two reasons why this would not be the case. First, using a small domain for the simulations is not necessarily representative for a bigger domain because of boundary effects. As the pore-network model is reduced in size, boundary effects will become relatively more important. The volume for which an increase in volume does not lead to different properties or results is called the Representative Elementary Volume (REV). Secondly, randomness is more important in a small domain than in a big domain. Using a different realization of the pore size distribution will lead to different results, even if all the constants remain unchanged. So if we obtain different results for different scenarios, we should check that this it not merely due to the utilization of different realisations of the pore size distribution.

REV. According to [13], the model size corresponding to an REV is 35x35x35 pores for the pore-network model used. [15] state that a 3D pore-network model must contain at least 15x15x15 pore bodies in order to appear statistically homogeneous. A 15x15x15 domain contains 3375 pores. Due to computational restrictions, we used a 10x10x30 model for this research, which contains only 3000

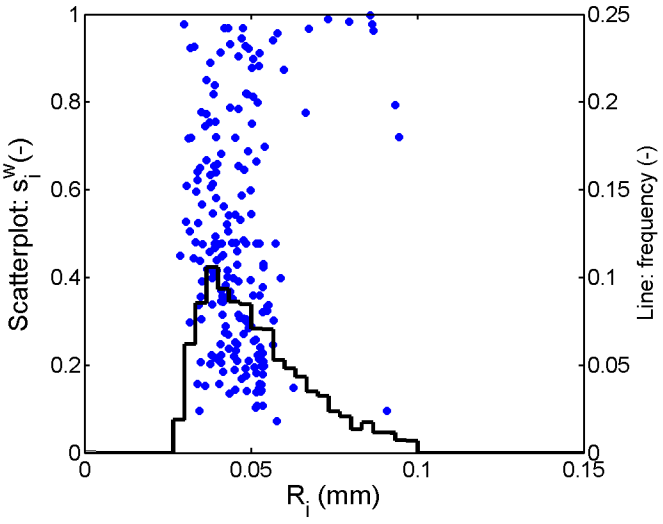

Figure 12: Scatterplot: every dot represents a pore body containing disconnected non-wetting phase. For every such pore body, the saturation of wetting phase can be read on the y-axis, and the radius of the pore body can be read on the x-axis. Line: pore size distribution of all 3000 pore bodies in the domain (radius). For a reference (scenario 1) 10x10x30 free imbibition run at $S^w = 0.8$.

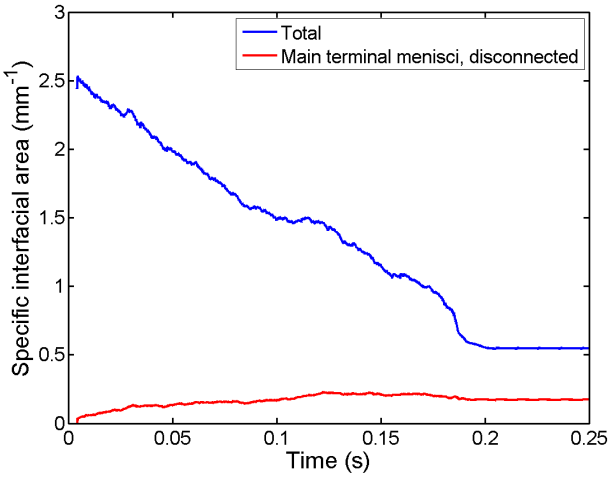

Figure 13: Total specific interfacial area (total interfacial area divided by total sample volume) and specific interfacial area of disconnected non-wetting phase (interfacial area due to disconected regions divided by total sample volume) in the domain. For a reference (scenario 1) 10x10x30 free imbibition run.

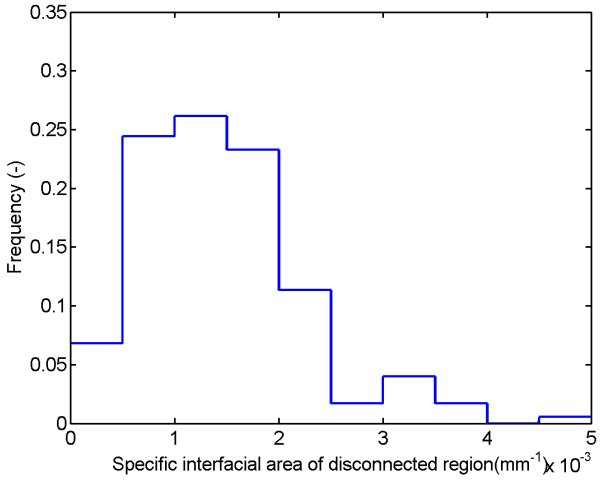

Figure 14: Frequency distribution of disconnected regions with a certain specific interfacial area (interfacial area of the disconnected region over total domain volume). For a reference (scenario 1) 10x10x30 free imbibition run at $S^w = 0.8$.

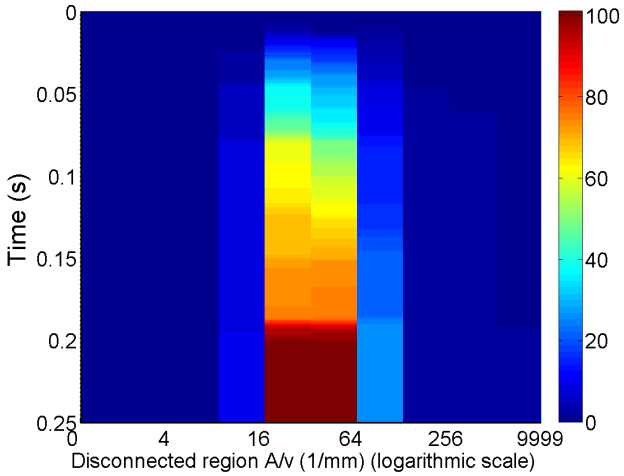

Figure 15: Interfacial area of disconnected region divided by the volume of that disconnected region. Colors correspond to number of occurences within a class. For a reference (scenario 1) 10x10x30 free imbibition run.

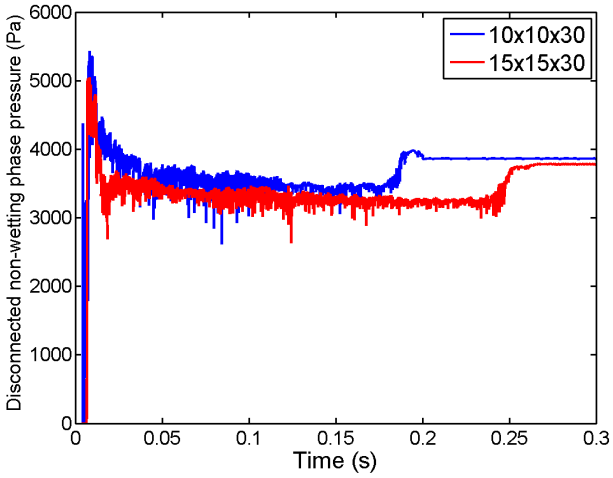

Figure 16: Average disconnected non-wetting phase pressure in time. For a 10x10x30 and a 15x15x30 free imbibition model run.

pores. Although the results may change when increasing the model size, it is unlikely that the qualitative behavior will change. This means we should not draw any quantitative conclusions from the results, but it may still be possible to draw qualitative conclusions from the results. The average disconnected non-wetting phase pressure for two different model sizes is shown in Figure 16. For both model runs, the reference scenario (scenario 1) parameters are used. The only difference is that for one model run 10x10x30 pores where used, while for the other 15x15x30 pores were used. Due to computational restrictions, the model size has not been increased more. We observe similar pressures during imbibition and during steady state for both models. The pressure does not follow a smooth line, but is rather noisy. The fact that we obtain similar results for the 10x10x30 model run as for the 15x15x30 model run tells us the model is not very sensitive to change in size at 10x10x30 pores. The noisy behavior is due to the fact that we are working in a small domain: when there is movement of fluids, it will have an effect on the pressures throughout the domain. If the domain is small, the effect is relatively large. Indeed, the bandwidth within which the values vary is smaller for the 15x15x30 model run. The bandwidth also decreases with time, since the amount of wetting fluid is increasing.

Utilization of different pore size realizations. Figure 17 shows results for four different realizations of the same pore size distribution for the reference scenario (scenario 1) and the increased pore throat size scenario (scenario 6). The number of disconnected regions is consistently lower and the total disconnected volume is consistently higher for the increased throat radius scenario. This means we can safely assume that different results for different scenarios are due to the changed parameters, and not due to the utilization of a different realization of the pore size distribution.

Unsmoothed and smoothed spatial distributions of pressures for the increased non-wetting phase scenario (scenario 4) are compared in Figure 18. The $P^{n,dis}$ values are more erratic when unsmoothed (Figure 18a) then when smoothed (Figure 18b). At distances 5, 17, 18 and 19, $P^{n,dis}$ equals zero for the unsmoothed graph. The one at distance 5 is located well upstream of the wetting front. In these slices, there is no disconnected non-wetting phase so a value of zero is plotted. For the smoothed graph, these slices do not have a value of zero. This is because each slice represents the average value calculated for the unsmoothed graph of three adjacent slices. This means that a slice containing no non-wetting phase will lower the average non-wetting phase pressure. Near the wetting front in Figure 18b, there seems to be a gradient in $P^{n,dis}$, while we do not observe this in Figure 18a if we disregard the slices which have

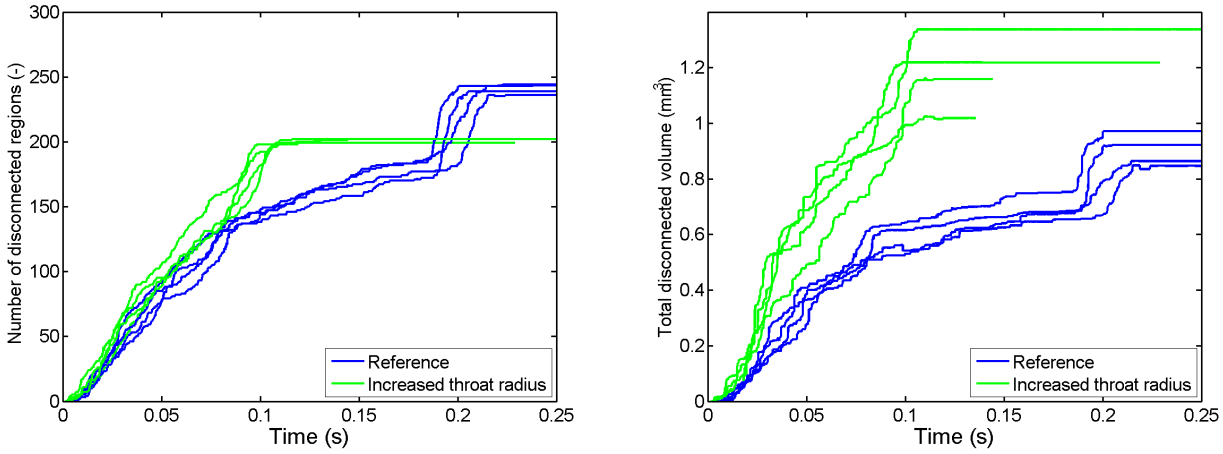

(a) (b)

Figure 17: Number of disconnected regions (a) and total disconnected non-wetting phase volume (b) for reference scenario runs (blue) and for increased pore throat radius scenarios (green).

a value of zero. The fact that there are some slices containing no non-wetting phase shows the effect of working in a small domain. If the domain size were to be increased, this would be less likely to happen. The gentle gradient in $P^{n,dis}$ in Figure 18 is the effect of the averaging algorithm, and does not have a physical meaning. However, we can still draw meaningful conclusions if we use the unsmoothed graphs and ignore the slices with a value of zero, since the slices around it give enough information about the spatial distribution of pressure.

Conclusions. From literature, it is clear that a 10x10x30 pore-network model is smaller than the REV. This means the results can change when increasing the model size. However, we judge it unlikely that the qualitative behavior will change. Some effects are observed which are related to working in a small domain. These include the noisy behavior of the average non-wetting phase pressure and the fact that some slices perpendicular to the flow direction contain no disconnected non-wetting phase even upstream of the wetting front. This means we should not draw any quantitave conclusions from our results. However, since changing the pore throat radius led to a consistently different result, we argue that we can draw qualitative conclusions from the results.

8.3 The influence of flow rate on trapping

One of the research questions is: What is the influence of the flow rate on trapping? Results for different flow rates are presented in this section. The flow rate has been varied by increasing the pressure of the non-wetting phase reservoir from 0Pa to 500Pa (scenario 2) and to 1000Pa (scenario 3). The same realization of the pore size distribution is used for the three models. We did not select a constant flux boundary condition because that would divide the flow equally over all pore bodies at the boundary. This would automatically lead to a regular or sharp front. Figure 19 shows the number of disconnected regions and the total disconnected non-wetting phase volume in time. For the $p^n = 0$Pa boundary condition (scenario 1), a constant value is reached the soonest. This corresponds with a higher flow rate since steady state is reached sooner. Scenario 2 has an intermediate flow rate, and scenario 3 has the lowest flow rate. Similarly, scenario 1 has the highest number of disconnected regions and total disconnected non-wetting phase volume, scenario 2 is intermediate and scenario 3 has the lowest number of disconnected regions and total disconnected non-wetting phase volume. Figure 20 shows that there is no consistent trend in the average disconnected non-wetting phase pressure. For all three scenarios, most disconnected regions

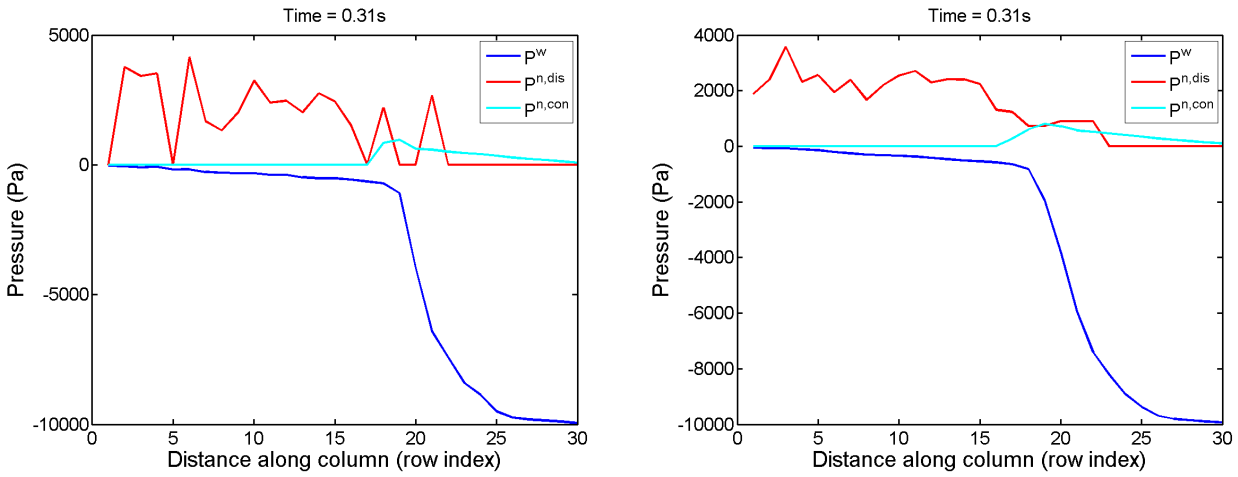

Figure 18: Unsmoothed (a) and smoothed (b) spatial distribution of pressure for a 10x10x30 free imbibition run. The $P^{n,dis}$ values in (a) which are zero correspond to 10x10 cross-sections which contain no disconnected non-wetting phase.

extend over only one pore body (figure not provided). Finally, we observe a sharper wetting front for lower flow rates (figure not provided).

Trapping is thus shown to decrease with a decreasing flow rate. A higher flow rate inhibits the formation of a stable arc meniscus in a pore throat, thereby decreasing the amount of snap-off. Also, disconnected regions are more mobile for high flow rates. We therefore expected trapping to increase with lower flow rates. The discrepancy between expectation and results may have a number of explanations.

1. The higher flow rate ensures a higher flow rate in the wetting films in the dry part of the domain. These may swell, causing snap-off to be more probable.

2. The flow in the flow direction is driven by suction, but is opposed by the increased non-wetting phase boundary pressure in scenario 3. Laterally though, the flow is driven only by suction. In other words, the pressure gradient is directional but suction is an isotropic force. So relatively, lateral flow will become more important. Any fingers developing will then be more quickly smoothed out. If the front is sharper, it also means that trapping is less likely.

3. We did not observe mobilization in our model runs. This does not mean that the model is incorrect, just that we did not use the right parameters for mobilization to occur.

4. Compared to models in literature, the pore-network model used for this research is more sophisticated because it uses a two-pressure algorithm, as opposed to a single-pressure algorithm. This allows effects such as counter-current flow to be taken into account.

5. The inhibition of the formation of a stable arc meniscus in a pore throat may not be explicitly incorporated in the pore-network model.

6. Most models use circular pore throats, so the snap-off condition is different than the condition used for this work.

We only investigated the cases of free imbibition and controlled imbibition. The case where the boundary conditions are adapted to increase the flow rate compared to free imbibition is called forced imbibition. For completeness, this case should be studied in future work. The wetting phase pressure

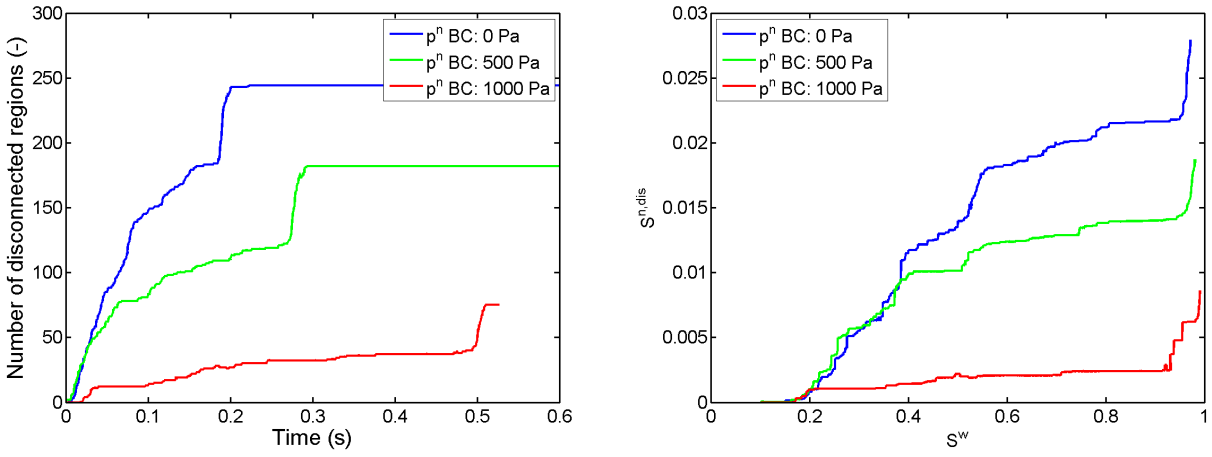

(a) (b)

Figure 19: Number of disconnected regions in time (a) and saturation of disconnected non-wetting phase vs saturation of wetting phase in the domain (b) for three different non-wetting phase boundary conditions: $0Pa$ (free imbibition, blue), $500Pa$ (controlled imbibition, green), and $1000Pa$ (controlled imbibition, red).

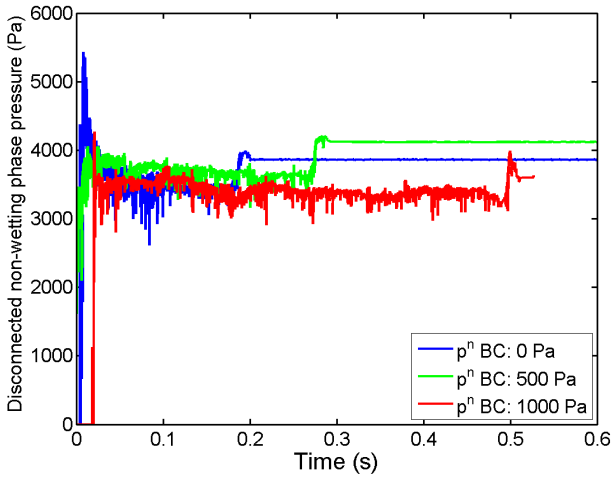

Figure 20: Average disconnected non-wetting phase pressure. For three 10x10x30 models with different non-wetting phase boundary conditions: $0Pa$ (free imbibition, blue), $500Pa$ (controlled imbibition, green), and $1000Pa$ (controlled imbibition, red).

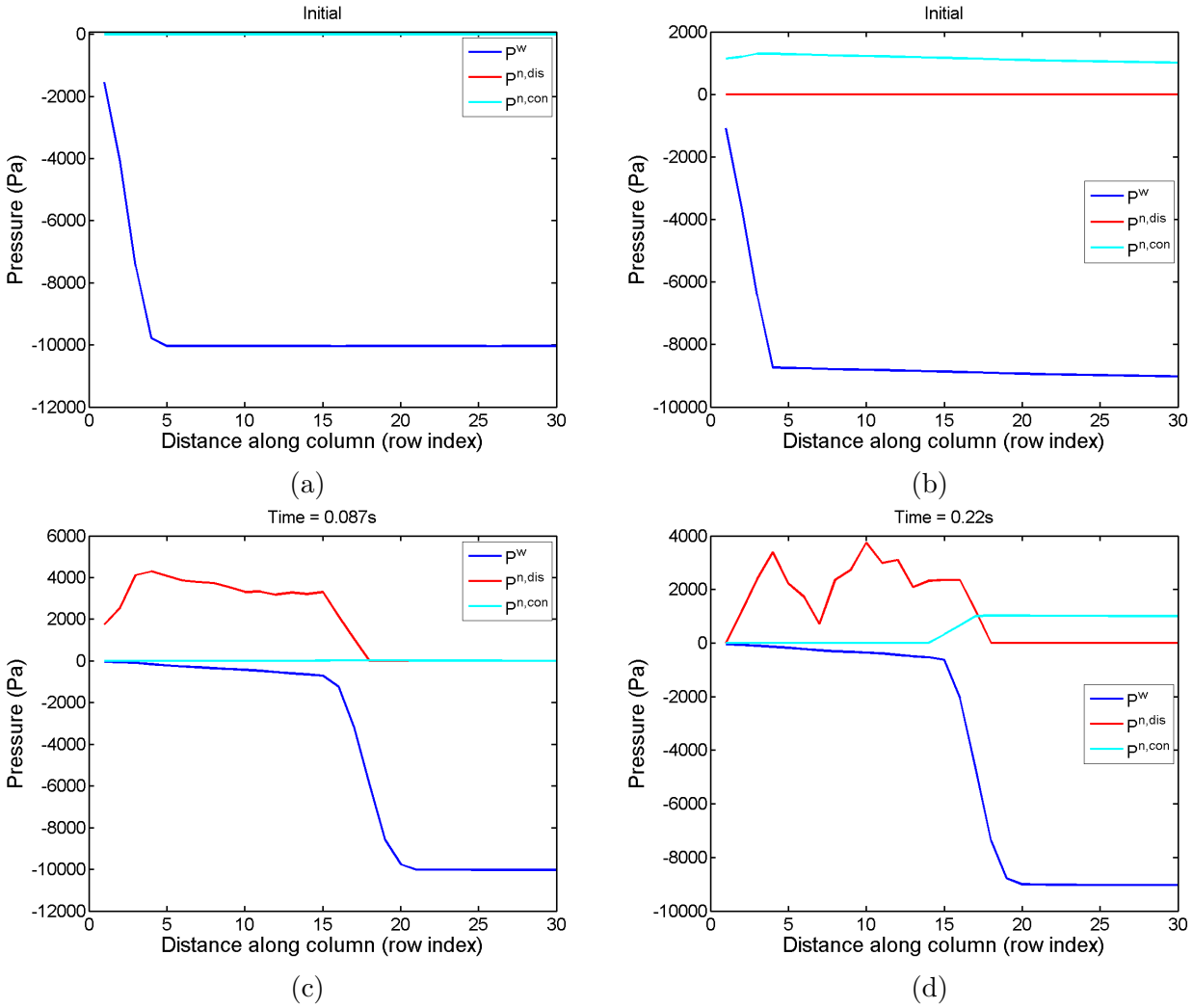

Figure 21: Spatial pressure distributions for two different non-wetting phase boundary conditions: 0Pa (free imbibition, a & c) and 1000Pa (controlled imbibition, b & d).

difference between upstream of the wetting front and downstream from the wetting front is just under 10000Pa for scenario 1 and just under 9000Pa for scenario 3 (Figure 21).

Conclusions. Decreasing the flow rate by increasing the non-wetting phase reservoir pressure during imbibition leads to sharper wetting fronts. This leads to a lower amount of trapping. Another reason why the amount of trapping decreases when decreasing the flow rate, is that wetting films in the dry part of the domain become smaller, thus decreasing the probability of snap-off.

8.4 The influence of non-wetting phase viscosity, variance in pore size and pore throat radius on trapping

One of our research questions is: What is the influence of non-wetting phase viscosity, variance in pore size and pore throat radius on trapping? Statistics about the number and size of disconnected regions for four scenarios (Section 7) are presented in this section to answer this question. In Section 8.1.3 we observed an initially high velocity of the wetting front. The velocity gradually decreases until the non-wetting phase boundary is reached, at which the velocity increases again. The slope in Figure 23a tells us how many disconnected regions are formed per unit time. A high slope corresponds to many newly

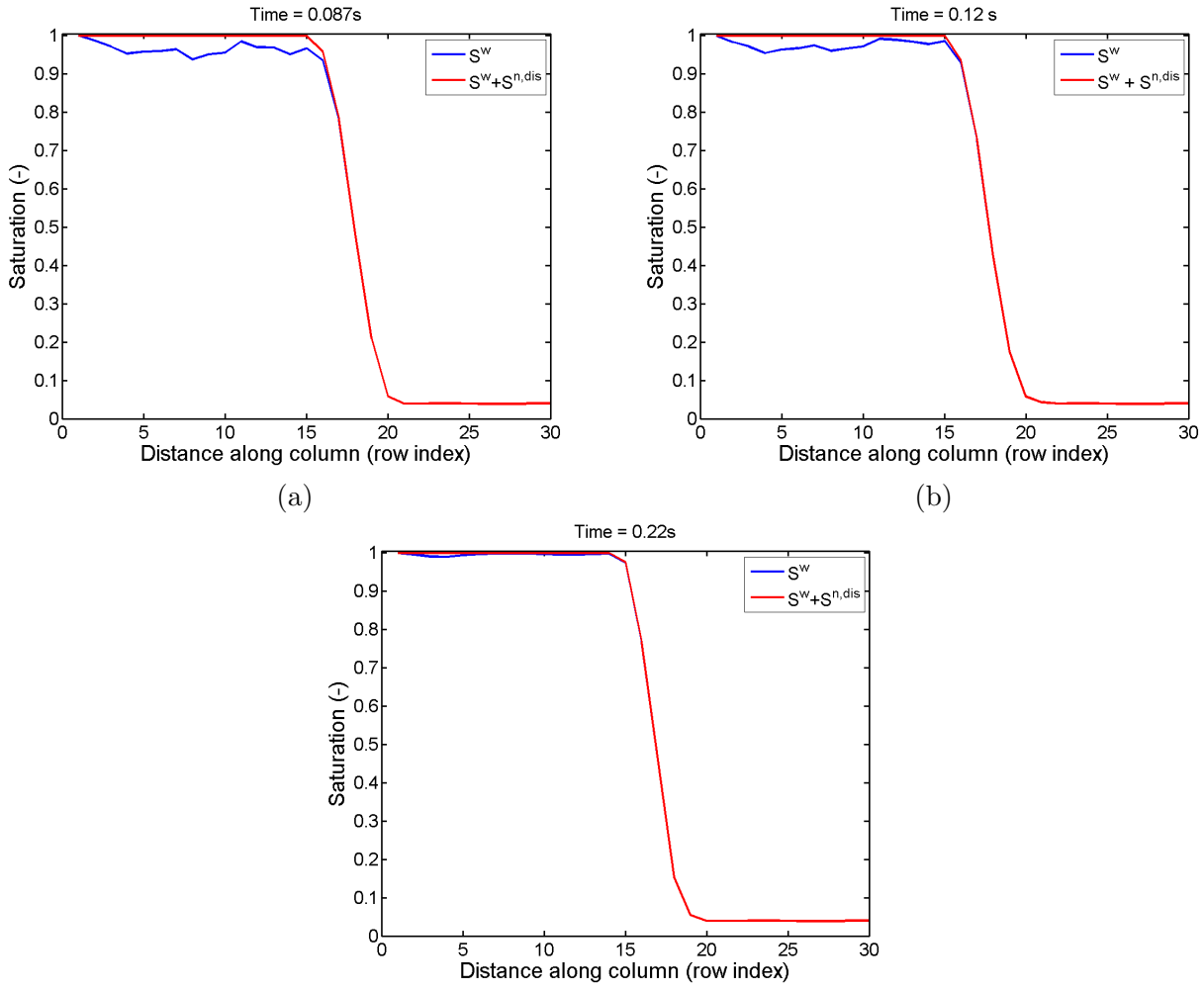

Figure 22: Saturation profile for three different non-wetting phase boundary conditions: (a) $p^n = 0Pa$, (b) $p^n = 500Pa$ and (c) $p^n = 1000Pa$.

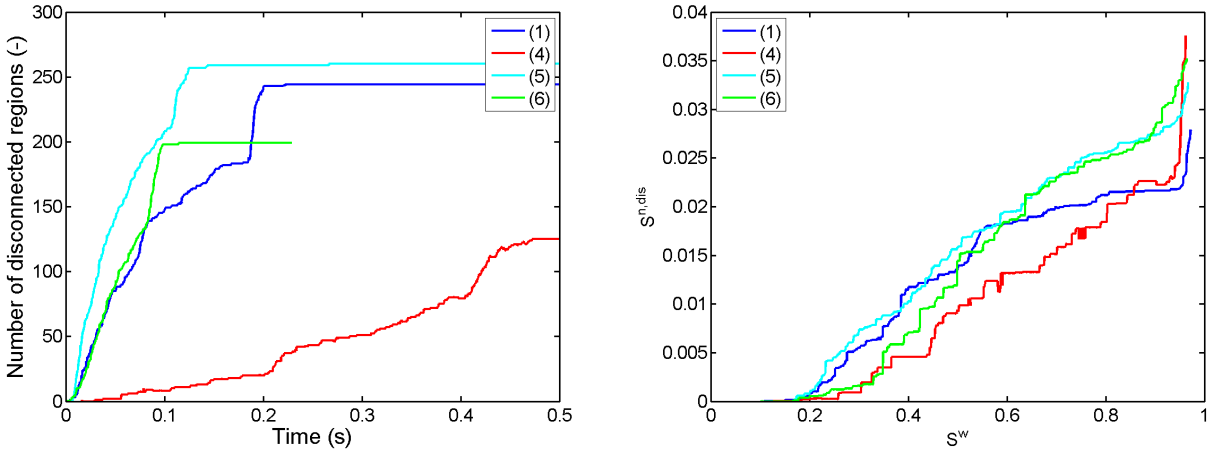

(a) (b)

Figure 23: Number of disconnected regions (a) and saturation of disconnected non-wetting phase in the domain (b) for four 10x10x30 free imbibition scenarios. **Blue**: (1) reference, **red**: (4) increased non-wetting phase viscosity, **cyan**: (5) Low variance in pore body radius and **green**: (6) increased pore throat radius.

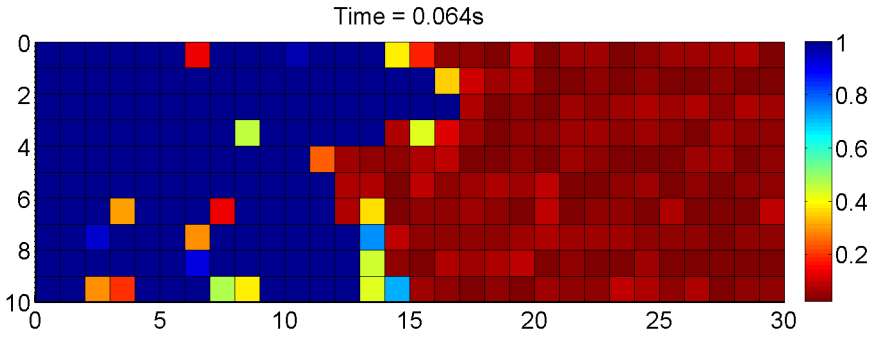

Figure 24: Saturation of wetting phase in a longitudinal cross-section of the middle of the domain for the reference scenario **(scenario 1)**. Every square corresponds to a pore body. For a 10x10x30 free imbibition run.

formed disconnected regions, and a low slope corresponds to few newly formed disconnected regions. Scenarios 1, 3 and 4 show a high slope initially, a gradually decreasing slope and finally a steep slope. This is similar to the wetting front velocity. Scenario 4 however, shows no gradually decreasing number of newly formed disconnected region, but rather a gradually increasing number. The slopes of scenarios 1, 3 and 4 in Figure 23b have a similar shape as in Figure 23a, except that here, we are plotting against the saturation. The $S^{n,dis}$ values start going up where $S^w \approx 0.2$. This corresponds to the intial saturation of water, both in the first two slices where for every pore body $s_i^w = 1$ and in the rest of the domain where $s_i^w \approx 0.05$. The slope reflects how much disconnected non-wetting phase is created in terms of how much the wetting phase saturation increases. Just after $S^w = 0.2$, where we know the velocity of the wetting front is high, there is a high slope and thus a high creation of disconnected non-wetting phase. After that, we know the velocity of the wetting front decreases, and we observe a gentler slope and thus less creation of disconnected non-wetting phase. This is consistent with our observations in 8.3.

Non-wetting phase viscosity (scenario 4). In order to assess the effect of non-wetting phase viscosity on trapping, we increased the non-wetting phase viscosity from $1.5 \cdot 10^{-5}$Pa s to $5 \cdot 10^{-4}$Pa s.

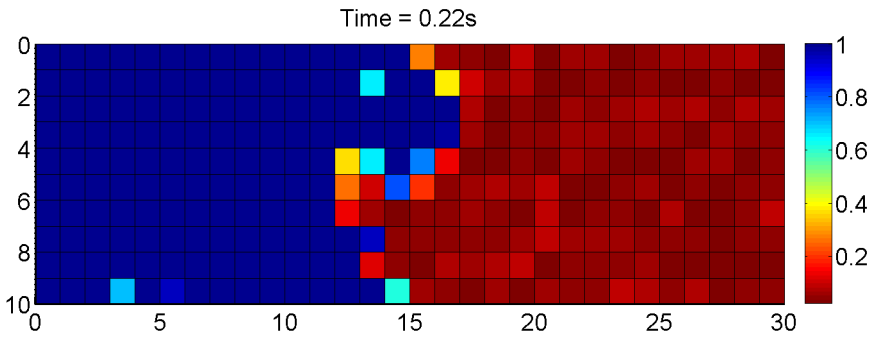

Figure 25: Saturation of wetting phase in a longitudinal cross-section of the middle of the domain for increased non-wetting phase viscosity **(scenario 4)**. Every square corresponds to a pore body. For a 10x10x30 free imbibition run. Uses the same realization of the pore size distribution as Figure 24.

The new value is half that of the wetting phase viscosity. Figure 23a shows that it takes 0.5s for this scenario to reach a constant value as opposed to 0.2s for scenario 1, so the flow rate is lower. Figure 23a also shows that the number of disconnected regions decreases for this scenario. Figure 23b shows that scenarios 1 and 2 have a similar final saturation, if the sharp saturation increase at $S^w \approx 0.95$ is not taken into account. We should not take this sharp increase into account because it is due to boundary effects. A similar residual saturation combined with a lower number of disconnected regions means that the disconnected regions should have a higher volume on average, which is confirmed in Figure 30. The average number of pore bodies over which a disconnected region extends is actually lower than for the reference scenario, i.e. it is still close to 1 (figure not provided). But, when taking the average of the s_i^w values of all the pore bodies containing disconnected non-wetting phase for steady state, we find a value of 0.47 for scenario 1, and a value of 0.61 for scenario 4. So generally, the saturation of non-wetting phase in a pore body containing disconnected non-wetting phase is lower for this scenario, but its volume is higher. This means that trapping must occur in bigger pore bodies, which is confirmed in Figure 26. In Figure 26, every dot represents a pore body containing disconnected non-wetting phase. For every pore body, its saturation of wetting phase can be read on the y-axis, and its pore body radius can be read on the x-axis. The blue dots, which correspond to the reference scenario (scenario 1) are mostly grouped between the values $0.03 < R_i < 0.06$. The red dots, which correspond to the increased non-wetting phase viscosity scenario (scenario 4), occur between the values $0.03 < R_i < 0.1$, so the average value for R_i is higher. Both the saturation of wetting phase and the pore body radius affect the capillary pressure (equation 17). An increase in s_i^w leads to a lower capillary pressure. A high pore body radius corresponds to a low capillary pressure. These two effects mean that for this scenario, the capillary pressure should be lower. Figure 27 shows that P^n is lower for this scenario. At steady state, P^w goes to zero for both scenario 1 and scenario 4 (figure not provided). So as we expected, the capillary pressure deceased for scenario 4.

A lower flow rate is to be expected, since there is more resistance to flow. The flow rate also has an influence on the trapping behavior (Section 8.3). Therefore, it is meaningful to compare this scenario to scenario 3, for which steady state is also reached at $t = 0.5$s. The flow rate of scenario 4 and scenario 3 are thus similar. The number of disconnected regions for scenario 4 is 80, and for scenario 3 it is 40 before the sharp increase in number of disconnected regions which is due to boundary effects. The disconnected non-wetting phase saturation for scenario 4 is 0.025 and for scenario 3 it is 0.0025 just before the sharp increase in saturation which is due to boundary effects. So the disconnected regions of scenario 4 can be compared to scenario 3 as follows: there are more disconnected regions, which still extend over only one pore body but have a higher volume and thus add up to a higher volume. The wetting front does not appear more fingered for this scenario. In order for viscous fingering to happen, the viscosity ratio should be higher than 1 [20]. From Section 4.5 we learned that a relatively high non-wetting phase viscosity

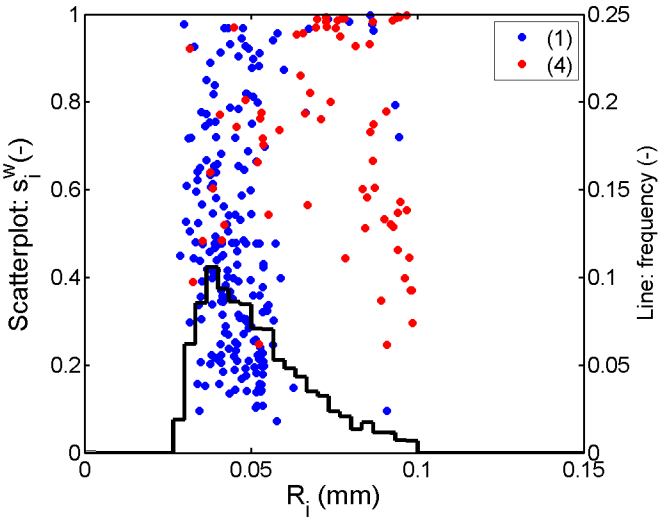

Figure 26: Scatterplot: every dot represents a pore body containing disconnected non-wetting phase. For every such pore body, the saturation of wetting phase can be read on the y-axis, and the radius of the pore body can be read on the x-axis. Line: pore size distribution of all 3000 pore bodies in the domain (radius). **Blue:** (1) reference, **red:** (4) increased non-wetting phase viscosity.

leads to a high residual non-wetting phase saturation. This is consistent with our comparison between scenario 4 and scenario 3. Since viscous fingering does not occur more for this scenario, we argue that trapping due to bypassing does not become more important for this scenario. This is consistent with the observation that like for scenario 1, disconnected regions extend over only one pore body.

Variance in pore size (scenario 5). This scenario uses a variance in pore body radius of 0.3mm^2, as opposed to 0.5mm^2 for the reference scenario. Figure 23a shows that a constant value for the number of disconnected regions is reached sooner for this scenario, so steady state is reached more quickly. Figure 23b shows that the residual saturation is higher for this scenario. The total pore volume for scenario 5 is 2.9mm^3 as opposed to 4.3mm^3 for scenario 1. The reason for this is that there is a cubic increase of pore volume with increasing pore radius. A high pore body radius will lead to an 'extremer' high pore body volume. In an absolute sense, a low pore body radius leads to a pore body volume which is less far from the volume a pore body has when it has the average pore body radius. Decreasing the variance in pore body radius takes out both big and small pore bodies, but the effect of taking out a large pore body on the mean volume is greater than the effect of taking out a small pore body. The fact that steady state is reached faster is due to the lower pore volume. It takes less long to fill a small volume than a large volume for the same flow rate so the velocity of the wetting front is higher even at the same volumetric flow rate. Although the residual saturation is higher, the total disconnected volume is lower for this scenario because the total pore volume is lower.

A possible explanation for the increased number of disconnected regions is that trapping preferentially occurs in pore bodies with a certain size. In Section 8.1.4 (Figure 12), we stated that trapping preferentially occurred in pore bodies with a radius below 0.06mm. Figure 28 shows the pore size distributions of all 3000 pores and the saturation and pore sizes of all pore bodies containing disconnected non-wetting phase for scenario 1 (Figure 28(a)) and scenario 5 (Figure 28(b)). The pore size distribution of scenario 5 is narrower since it has a decreased variance. For this scenario, there are more pore bodies with a volume below 0.06mm than for scenario 1 which favors the amount of trapping, which may be the explanation for the increased number of disconnected regions for scenario 5.

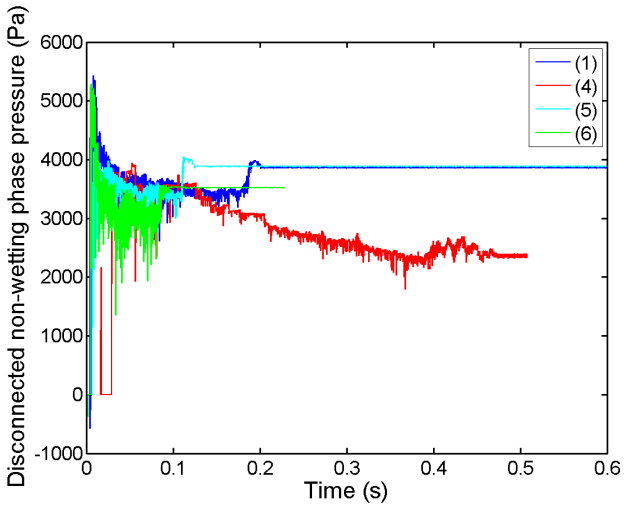

Figure 27: Average disconnected non-wetting phase pressure for four 10x10x30 free imbibition scenarios. **Blue**: (1) reference, **red**: (4) increased non-wetting phase viscosity, **cyan**: (5) Low variance in pore body radius and **green**: (6) increased pore throat radius.

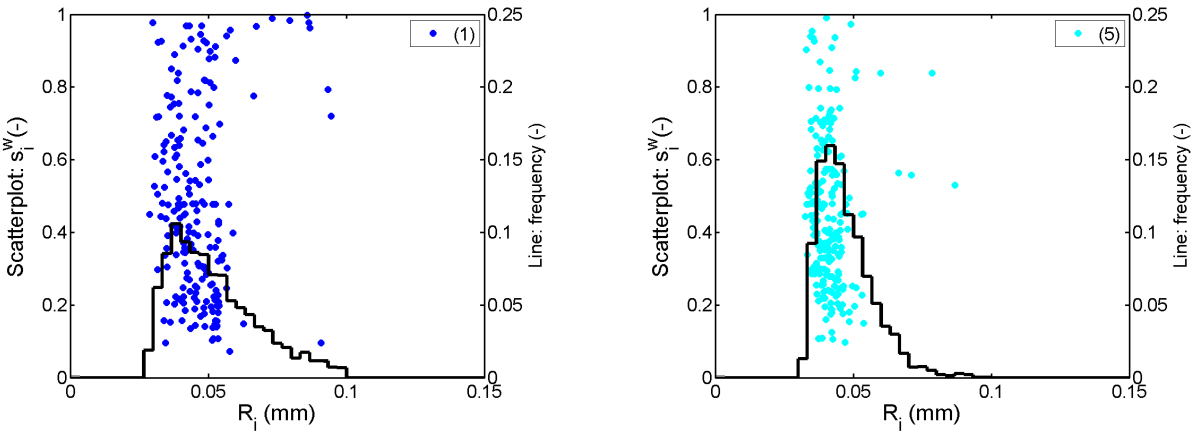

(a) (b)

Figure 28: Scatterplot: every dot represents a pore body containing disconnected non-wetting phase. For every such pore body, the saturation of wetting phase of that pore body can be read on the y-axis, and the radius of the pore body can be read on the x-axis. Line: pore size distribution of all 3000 pore bodies in the domain (radius). For a reference (scenario 1) 10x10x30 free imbibition run. **(a):** (1) reference, **(b):** (5) decreased variance in pore radius.

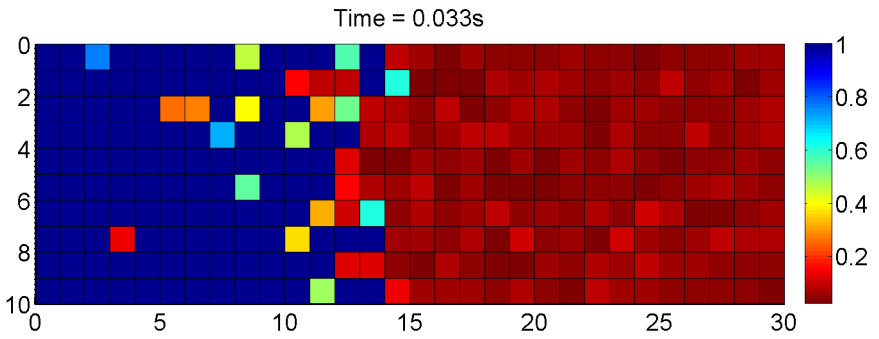

Figure 29: Saturation of wetting phase in a longitudinal cross-section of the middle of the domain for increased pore throat radius **(scenario 6)**. Every square corresponds to a pore body. For a 10x10x30 free imbibition run.

From Figure 30, we observe that the variation in disconnected region volume is less than for the reference scenario. This shows that the volume of disconnected regions depends on the pore size distribution.

Pore throat radius (scenario 6). In order to assess the effect of the pore throat radius on trapping, the pore throat radius is increased by a factor of 1.25. Since the pore throats have no volume in the pore-network model, this does not influence the total pore volume. Figure 23a shows that steady state is reached more quickly than for the reference scenario. There is a decrease in number of disconnected regions, and an increase in saturation of trapped phase (Figure 23b). This means that the disconnected regions have a higher volume on average, which is confirmed in Figure 30. In contrast to scenario 4, the disconnected regions do extend over more pore bodies than for the reference scenario. Although the higher residual saturation may be due to the higher flow rate, we do not observe the higher number of disconnected regions which would be expected for higher flow rates. The disconnected regions can be compared to those of the reference scenario as follows: there are less disconnected regions which have a bigger volume, extend over more pore bodies and add up to a higher total volume. Since the conductivity of a pore body depends on r_{ij}^4 (equations 10, 13 and 14), a larger pore throat leads to a higher conductivity. Therefore, the flow rate is higher, and steady state is reached more quickly.

The decreased number of disconnected regions and increased total volume may have to do with the changed flow dynamics. Firstly, trapping due to bypassing of the non-wetting phase by the wetting phase occurs because of local differences in conductivity (Section 4.5). Because the conductivity is increased for this scenario, this effect may be stronger. This leads to more trapping due to bypassing, and more extensive disconnected regions which is consistent with our observations. Figure 30 indicates that the number of 'big' disconnected regions ($> 0.0032\text{mm}^3$) is higher for this scenario. Secondly, equation 18 shows that the probability of snap-off decreases for a higher pore throat radius. The number of disconnected regions should then go down. On the other hand, increased flow rate should lead to a higher number of disconnected regions. But since the number of disconnected regions goes down, the first effect is more important for this scenario. We conclude that trapping due to bypassing has become more important, while trapping due to snap-off has become less important. These conclusions are similar to those in [15].

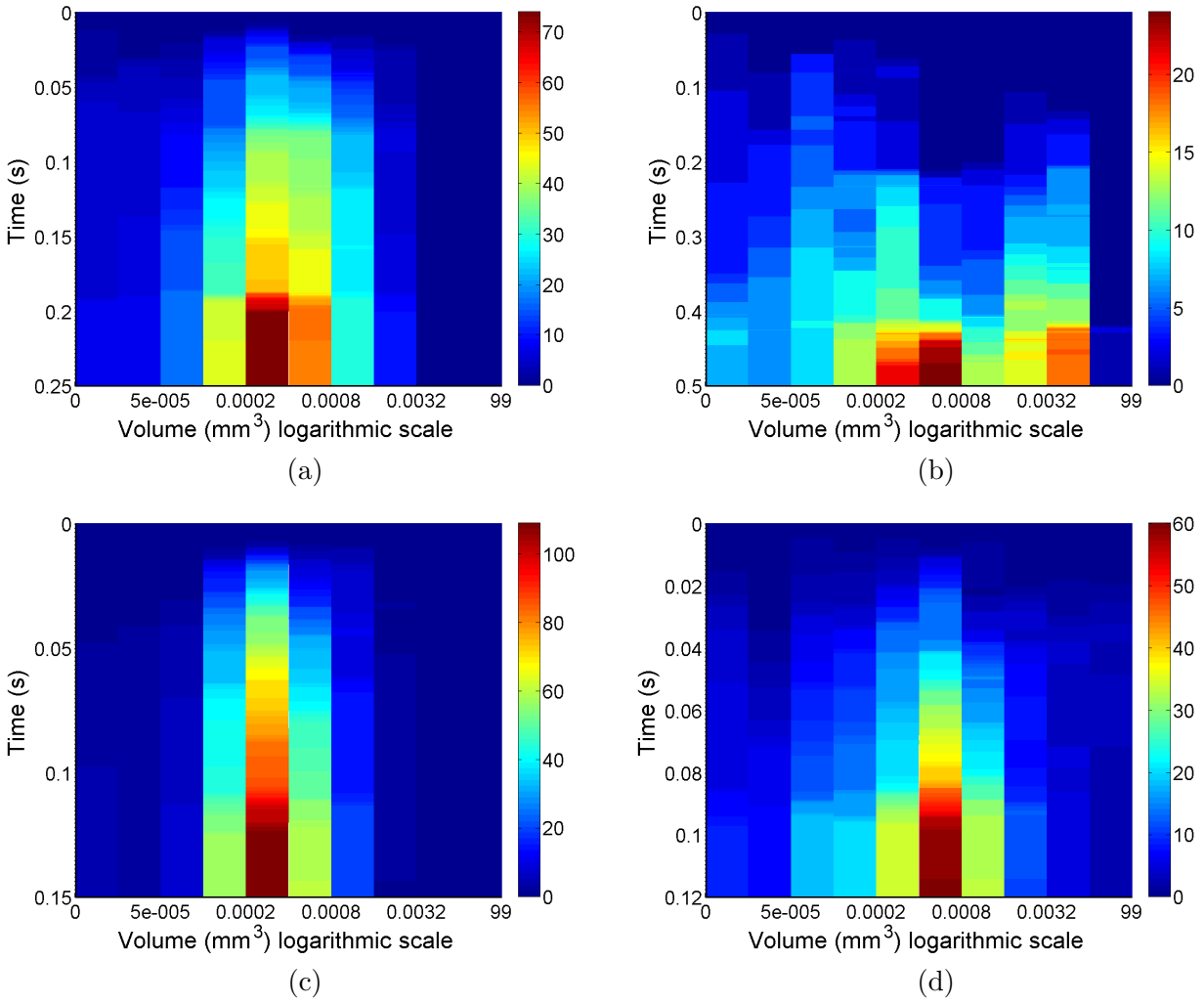

Figure 30: Colorplot of the evolution in time of the size distribution of disconnected regions for different scenarios, for 10x10x30 free imbibition model runs. Colors correspond to the number of occurences within a class. a) Reference, b) Increased non-wetting phase viscosity, c) Decreased variance in pore body size, d) Increased pore throat size. Color corresponds to number of occurrences within a class.

9 Conclusions

Trapping during imbibition can occur due to the snap-off of a single pore, or due to bypassing of the non-wetting fluid by the wetting fluid. The second mechanism occurs because fluid will flow faster in some pores than in others since pore sizes are distributed randomly. The wetting fluid thus has the possibility to flow around a non-wetting phase region and surround it completely. This mechanism is strongest when the wetting front is irregular. If the second mechanism is important, the disconnected regions tend to extend over more pore bodies than if the first mechanism is important. Compared to literature, low residual saturations were found. This may be due to the fact that most literature focuses on water-oil systems while our simulations are for water-air systems. Also, our simulations were done in a small domain with low viscosity ratios with a constant coordination number of 6. In contrast to what was expected from literature, lower flow rates led to lower trapping. This was due to the wetting front becoming sharper, and possibly that wetting films became smaller, thereby decreasing the probability of snap-off. Also, the inhibition of the formation of a stable arc meniscus in a pore throat may not be explicitly included in the pore-network model. Increased non-wetting phase viscosity led to lower flow rates. At an unchanged flow rate, increased non-wetting phase viscosity led to a higher number of disconnected regions, a higher residual saturation, a higher average volume of disconnected regions and caused trapping to occur in bigger pore bodies. For this scenario, snap-off of a single pore became more important. Another parameter which was assessed was the variance in the pore size. Decreasing the variance in pore body radius led to a lower pore volume. This led to a higher wetting front velocity. The variance in volume of disconnected regions also decreased. This means that the volume of disconnected regions depends on the pore body size. Increasing the pore throat radius led to a higher wetting front velocity since the conductivity of the pore throats went up. This led to a more fingered front. Consequently, trapping due to bypassing was important and the disconnected regions extended over more pore bodies. On the other hand, the increased pore throat radius led to a lower probability of snap-off. This decreased the total number of disconnected regions. So trapping due to snap-off of a single pore was less important and trapping due to bypassing was more important for this scenario.

10 Future work

- The same methods used in this research can be applied to study the effect of contact angle and initial wetting phase saturation on trapping. It has been shown that the effect of contact angle on trapping is significant in [4, 6, 7, 11, 15, 20]. The initial saturation determines the size of the wetting films initially present in the domain. Since snap-off is related to the swelling of the wetting films, the initial saturation may be an important parameter for trapping.

- Low residual saturation values were found in this work compared to literature. A possible explanation is that most literature focuses on brine-oil systems instead of water-air systems. Therefore, for comparison with other studies it is recommended to study a brine-oil case using the methods presented in this work.

- For this research, no simulations have been done where the viscosity of the non-wetting phase μ^n exceeds the viscosity of the wetting-phase μ^w. This case should be studied, since it has been shown that viscous fingering takes place when $\mu^n > \mu^w$ holds [20].

- More simulations need to be run, since many factors act in synergy: the effect of capillary number is much more significant for higher aspect ratios due to the suppression of snap-off [15], the effect of capillary number on residual saturation decreases with the decrease of viscosity ratio [6] and contact angle and viscosity are not independent [20].

- In [13], it is stated that a pore-network model of 35x35x35 pores corresponds to the REV. For this work, we used a 10x10x30 model, so only qualitative conclusions were drawn. If more quantitative conclusions are required, the model size should be increased to 35x35x35.

- The development of the post-processor was the first step toward studying the evolution of individual disconnected regions in time. Although it distinguishes disconnected regions, it does not track the regions in time. An algorithm should be developed which does have this option. This will provide insight into what factors influence breakup and mobilization of disconnected regions.

The most straightforward of these options are applying the same methods as were used in this research to run models with a changed contact angle or initial saturation, an unfavorable viscosity ratio and a brine-air system. Assessing the effect of capillary number, aspect ratio, viscosity ratio and contact angle in synergy is more intensive because it requires many simulations, but if done in a 35x35x35 model may be eventually used to come up with empirical relations to predict residual saturations. These options do not necessarily involve the development of new methods. Developing an algorithm to track the disconnected regions does, but will improve insight specifically into the breakup and mobilization of disconnected regions.

A Instructions concerning the pore-network model

The pore-network model used for this research is designed by [13]. It is a Fortran code. After we have compiled it to Main_Imbibition.exe, we have to take the following steps to run the model:

1. Create a new folder
2. Place Main_Imbibition.exe and input.txt in the folder
3. Adjust the input file
4. Run the model
5. Stop the model using Ctrl + C when the message 'All pore throats at the lower boundary have snapped off' is displayed. This may take 1 to 2 hours for a 10x10x30 model on a 2.33 GHz computer.

Consider a pore-network model with nx x ny x nz pores. The nz pores are in direction of the flow. Snapshots are generated for every time step in the following folders:

1. PN. The non-wetting phase pressure. One ASCII file per time step with nx x ny reals.
2. SW. The wetting phase saturation. One ASCII file per time step with nx x ny reals from 0 to 1
3. tube. The filling of the pore throats. One ASCII file per time step with [(nx x ny x nz)+ nx x ny = number of throats] booleans for a periodic boundary condition. If there is only wetting phase in a tube, the value is 0. If there is both wetting and non-wetting phase, the value is 1.

The pore chambers are ordered first in the nx direction, then in the ny direction and finally in the nz direction. So if (x,y,z)=(2,1,1), this is pore body number 2 and is the second value in the PN and SW file. . For a 10x10x30 model, (1,2,1) is number 11, and (1,1,2) is number 101. The same numbering scheme is used for pb2pth.txt and pore_dist.txt (Table A). The numbering of the pore throat is given in the pth2pb.txt file. The most important output files which are generated only once for the model are:

generalinfo.txt gives the parameters which were used for the simulation

interfacial_area.txt contains 4 columns of integers with 1 line for every timestep. The columns represent: 1) time, 2) interfacial area of corner interfaces, 3) interfacial area of main terminal meniscii, 4) Wait for confirmation Vahid: disconnected corner interfaces??.

pb2pth.txt contains nx x ny x nz rows with 6 integers for a periodic boundary condition. The row number corresponds to the pore number. The integers correspond to the pore throat number to which it is connected.

pore_dist.txt contains nx x ny x nz reals. Gives the DIAMETER of the pore bodies in mm.

pth2pb.txt contains (nx x ny x nz)*3 + nx x ny rows. Each row corresponds to a pore throat and contains 1 (for the throats at the boundaries) or 2 (for all other throats) integers. The row number corresponds to the throat number. The integer corresponds to the pore body to which it is connected. Pore throats 1 until nx x ny correspond to the wetting phase boundary, where pore throat 1 is connected to pore body 1 and the wetting phase boundary, pore throat 2 is connected to pore body 2 and the wetting phase boundary, etc.. Pore throats (nx x ny x nz)*3 until (nx x ny x nz)*3 + nx x ny are connected to the non-wetting phase boundary. For these pore throats, the pore throat with the highest number is connected to the non-wetting phase boundary and the pore body with the highest number, the pore throat with the second-to-highest number is connected to the non-wetting phase boundary and the pore body with the second-to-highest number, etc.

The input file is mostly self-explanatory. For using the model with a specified pore size distribution and for using the model with a specified initial saturation, more explanation is needed.

Using a specified pore size distribution. In this case the "generator= !if generator =1: it generates a new pore distribution,!else it uses a file" should be set to 0. Then, the program will use the pore_dist.txt file which is in the result_folder will be used. Vahid confirm: The pore throat sizes depend on the pore body sizes and therefore do not need to be specified.

Using a specified initial saturation. First, the "!starting with an initial saturation, if ==1, there is a start not equal to one!" line in the input.txt file should be set to 1. Second, a TubePhase.txt and a sat.txt file need to be placed in the same directory as where Main_imbibition.exe is located. These should have the same format as the tube and SW ASCII files (Table 3) and serve the same function.

B Pseudocode of the post-processor CSDA

Main code For a 10x10x30 model.

- calculate total pore volume
- WRITE total pore volume (vporetot)
- DO timestep=1:maxtimestep
  - DO $a = 3000, 2901, -1$!Find connected non-wetting phase
    - IF pore body a contains n phase, has not been checked before and is connected to non-wetting phase reservoir through a pore throat
      - CALL subroutine checkbody; assign -1, retrieve number of pore bodies containing connected non-wetting phase and the total volume of connected non-wetting phase
  - $b = 0$
  - DO $a = 1, 3000$!Find disconnected non-wetting phase
    - if pore body a contains non-wetting phase and has not been checked before
      - $b = b + 1$
      - CALL checkbody, assign b, retrieve number of pore bodies in this disconnected region, the volume of this disconnected region, extreme coordinates for elongatedness and interfacial area of this disconnected region.
      - update matrices containing size, elongatedness, interfacial area and number of pore bodies for this disconnected region
  - WRITE matrices containing size, elongatedness, interfacial area and number of pore bodies for this disconnected region
  - WRITE Average disconnected non-wetting phase pressure for this timestep.
  - calculate longitudinal cross section values for the longcross file.
  - DO i=1,30 !determine spatial statistics for every slice (unsmoothed)
    - calculate pore volume in slice
    - calculate number of pore bodies containing disconnected non-wetting phase
    - calculate wetting phase volume and disconnected non-wetting phase volume in the slice
    - add all non-wetting phase pressure values for pore bodies containing disconnected non-wetting phase
    - add all non-wetting phase pressure values for pore bodies containing connected non-wetting phase
    - add all wetting phase pressure values
    - calculate S^w, $S^{n,dis}$ and $S^{n,con}$ by dividing by pore volume
    - calculate P^w, $P^{n,dis}$ and $P^{n,con}$ by dividing by 100, number of pore bodies containing disconnected non-wetting phase and number of pore bodies containing connected non-wetting phase respectively
  - DO i=1,1 !determine spatial statistics for slice 1 (smoothed)
    - calculate total pore volume in the first two slices
    - calculate wetting phase volume and disconnected non-wetting phase volume in the two slices
    - calculate S^w, $S^{n,dis}$ and $S^{n,con}$ by dividing by pore volume
    - calculate P^w, $P^{n,dis}$ and $P^{n,con}$ by averaging the unsmoothed values of the first two slices

- DO i=2,29 !determine spatial statistics for slices 2 to 29 (smoothed)
  - calculate total pore volume in slices $a-1$, a and $a+1$
  - calculate wetting phase volume and disconnected non-wetting phase volume in slices $a-1$, a and $a+1$
  - calculate S^w, $S^{n,dis}$ and $S^{n,con}$ by dividing by pore volume
  - calculate P^w, $P^{n,dis}$ and $P^{n,con}$ by averaging the unsmoothed values of the slices $a-1$, a and $a+1$
- DO i=30,30 !determine spatial statistics for slice 30 (smoothed)
  - calculate total pore volume in the last two slices
  - calculate wetting phase volume and disconnected non-wetting phase volume in the last two slices
  - calculate S^w, $S^{n,dis}$ and $S^{n,con}$ by dividing by pore volume
  - calculate P^w, $P^{n,dis}$ and $P^{n,con}$ by averaging the unsmoothed values of the last two slices

SUBROUTINE Checkbody

- calculate non-wetting phase volume in the pore
- add this volume to the non-wetting phase volume in the disconnected region
- CALL Indexpore to retrieve (x, y, z) index of the pore
- Compare to maximum and minimum indices of previous pore bodies in this disconnected region and replace if necessary
- assign number to this pore body (-1 for connected non-wetting phase, number of disconnected region for disconnected non-wetting phase)
- CALL Interfar to calculate interfacial area in this pore
- Add interfacial area of this pore to interfacial area of other pores in this disconnected region
- DO for all pore throats connected to this pore body
  - IF there is non-wetting phase in this pore throat and it is not connected to a reservoir
    - CALL Checkthroat

SUBROUTINE Checkthroat

- DO a=1,2 ! for the two pore bodies which the throat connects
  - IF pore body a has not been checked before
    - number of pore bodies for this disconnected region is increased by 1
    - CALL Checkbody (if a throat contains non-wetting phase, the two pore bodies it connects also contain non-wetting phase)

SUBROUTINE Indexpore

- calculate the x,y and z indices of a pore body based on its number

SUBROUTINE Interfar

- calculate interfacial area of the pore body

C Output files of the post-processor CSDA

The format and description of the output files of CSDA is given here. If a file has 405x1000 values, 405 corresponds to the number of columns, and 1000 corresponds to the number of lines. The number of lines is often the number of timesteps, this is indicated with ...x(ntimesteps). All output files are ASCII files.

Folder: Out Contains an ASCII file for every time step. Every file has 30000 integers which correspond to the pore bodies. If the value is 0, then there is no non-wetting phase in the pore body. A value of -1 means that there is connected non-wetting phase in the pore body. A value greater than 0 indicates the number of the disconnected region.

Folder: PW Contains an ASCII file for every time step. Every file has 3000 reals which correspond to the wetting phase pressure in the pore body.

bubelong contains 405x(ntimesteps) reals. On every line, there is a value for each disconnected region of the last time step. If there are 220 disconnected regions, the right 180 values are equal to zero. The value corresponds to the elongatedness of a disconnected region. If there are more than 405 disconnected regions for a time step, an error will occur.

bubnbod contains 405x(ntimesteps)reals. On every line, there is a value for each disconnected region of that time step. If there are 220 disconnected regions, the right 180 values are equal to zero. The value corresponds to the number of pore bodies over which the disconnected region extends. If there are more than 405 disconnected regions for a time step, an error will occur.

bubsAi contains 405x(ntimesteps) reals. On every line, there is a value for each disconnected region of that time step. If there are 220 disconnected regions, the right 180 values are equal to zero. The value corresponds to the interfacial area of the region over the volume of that region. If there are more than 405 disconnected regions for a time step, an error will occur.

bubsAidom contains 405 reals. There is a value for each disconnected region of the last time step. If there are 220 disconnected regions, the right 180 values are equal to zero. The value corresponds to the interfacial area of the region over the total volume of the domain (pore space as well as solid matrix). If there are more than 405 disconnected regions for a time step, an error will occur.

bubsize contains 405x(ntimesteps) reals. On every line, there is a value for each disconnected region of that time step. If there are 220 disconnected regions, the right 180 values are equal to zero. The value corresponds to the volume of the disconnected region. If there are more than 405 disconnected regions for a time step, an error will occur.

disbodR contains as many reals as there are pore bodies containing disconnected non-wetting phase. Every value corresponds to the pore body radius (mm) of a pore body containing disconnected non-wetting phase for the last time step.

disbodSW contains as many reals as there are pore bodies containing disconnected non-wetting phase. Every value corresponds to the saturation of wetting s_i^w in a pore body containing disconnected non-wetting phase for the last time step.

longcross contains 10x30 reals between 0 and 1. Gives the saturations of the pore bodies in the 5th row. Only for the last timestep.

nbodiescon contains (ntimestep) integers. For every time step, the value corresponds to the number of pore bodies containing connected non-wetting phase. **Important:** at low $S^{n,con}$, this does not work well. There may be multiple regions of connected non-wetting phase, but nbodiescon only contains the number of pore bodies in the last connected region assessed.

nbubbles contains (ntimestep) integers. For every time step, the value corresponds to the number of disconnected regions

pnav contains (ntimestep) integers. Fore every time step, the value correspond to the average disconnected non-wetting phase pressure in the domain.

spatPNcon contains 30x(ntimesteps) reals. For every time step, contains values for 30 slices perpendicular to the flow direction. Values correspond to the average connected non-wetting phase pressure in that slice.

spatPNcon3smo contains 30x(ntimesteps) reals. For every time step, contains values for 30 slices perpendicular to the flow direction. Values correspond to the smoothed connected non-wetting phase pressure of that slice.

spatPNdis contains 30x(ntimesteps) reals. For every time step, contains values for 30 slices perpendicular to the flow direction. Values correspond to the average disconnected non-wetting phase pressure in that slice.

spatPNdis3smo contains 30x(ntimesteps) reals. For every time step, contains values for 30 slices perpendicular to the flow direction. Values correspond to the smoothed disconnected non-wetting phase pressure of that slice.

spatPW contains 30x(ntimesteps) reals. For every time step, contains values for 30 slices perpendicular to the flow direction. Values correspond to the average wetting phase pressure in that slice.

spatPW3smo contains 3x(ntimesteps)0 reals. For every time step, contains values for 30 slices perpendicular to the flow direction. Values correspond to the smoothed wetting phase pressure of that slice.

spatSNcon contains 30x(ntimesteps) reals between 0 and 1. For every time step, contains values for 30 slice perpendicular to the flow direction. Values correspond to the average connected non-wetting phase saturation of that slice.

spatSNcon3smo contains 30x(ntimesteps) reals between 0 and 1. For every time step, contains values for 30 slices perpendicular to the flow direction. Values correspond to the smoothed connected non-wetting phase saturation of that slice.

spatSNdis contains 30x(ntimesteps) reals between 0 and 1. For every time step, contains values for 30 slice perpendicular to the flow directions. Values correspond to the average disconnected non-wetting phase saturation of that slice.

spatSNdis3smo contains 30x(ntimesteps) reals between 0 and 1. For every time step, contains values for 30 slices perpendicular to the flow direction. Values correspond to the smoothed disconnected non-wetting phase saturation of that slice.

spatSW contains 30x(ntimesteps) reals between 0 and 1. For every time step, contains values for 30 slices perpendicular to the flow direction. Values correspond to the average wetting phase saturation of that slice.

spatSW3smo contains 30x(ntimesteps) reals between 0 and 1. For every time step, contains values for 30 slices perpendicular to the flow direction. Values correspond to the smoothed wetting phase saturation of that slice.

vcontot contains (ntimesteps) reals. Values correspond to (total connected non-wetting phase volume)*8 of the time step.

vdistot contains (ntimesteps) reals. Values correspond to (total disconnected wetting phase volume)*8 of the time step

vporetot contains 1 real. Value corresponds to total pore volume.

D Matlab scripts for plotting

To use the matlab scripts, the output files of each scenario should have the scenario name added behind the file name. For example, if the scenario is called 101030v, pnav becomes pnav101030v. For the list below, it is assumed that all output files of CSDA are thus named and present in a folder where Matlab can find them. **IMPORTANT:** the file 'interfacial_area.txt' should be renamed to for example 'interfacial_area101030v.txt' and should also be placed in this folder. It is contains links time steps to time in seconds and is used to plot graphs with time on the x-axis.

plotall calls most other scripts to automatically save various figures. **IMPORTANT:** only works if there are no other figures open: it saves only the figure called figure 1. The figure names will contain the scenario name. A number of parameters have to be defined in the script:

1. maxt: The maximum time, to adjust the time axis
2. eartimestep: the early time step for which spatial distributions of saturations and pressures will be plotted
3. midtimestep: the middle time step for which spatial distributions of saturations and pressures will be plotted
4. maxtimestep: the time step for steady state for which spatial distribution of saturations and pressures will be plotted

stansave. Input: (figure number and file name). Saves the specified figure in .png, .eps and .fig format

plotdiscon. Input:(scenario). plots $S^{n,dis}$ vs S^w

vdistotovervolw. Input: (scenario, maxt). Plots $\frac{V^{n,dis}}{V^w}$ vs time

plotvolumes. Input: (scenario, maxt). Plots $V^w, V^{n,dis}$ and $V^{n,con}$ vs time.

plotinterfar. Input: (scenario, maxt). Vahid should confirm: Plots total interfacial area, and interfacial area due to corner interfaces of disconnected non-wetting phase??

plotspat. Input: (scenario, timestep, '' or '3smo', 1 (for plotting at maximum time step) or 0 (for all other plots)). Plots the spatial distribution of saturations. When '' it plots unsmoothed distributions, when '3smo' it plots distributions which are smoothed over 3 slices.

plotspatP. Input: (scenario, timestep, 1 (for plotting at maximum time step) or 0 (for all other plots), '' or '3smo'). Plots the spatial distribution of pressures. When '' it plots unsmoothed distributions, when '3smo' it plots distributions which are smoothed over 3 slices.

plothist. (Scenario, number from 1 to 4, maxt). Plots evolution in time of distribution of specified variable.

1= Volume of individual disconnected regions

2= Elongatedness of individual disconnected regions

3= Specific interfacial area of individual disconnected regions: Their interfacial area divided by their volume.

4= Number of pore bodies of individual disconnected regions

plottempspat. Input: (scenario, maxt, variable, title, '' or '3smo'). Plots the unsmoothed ('') or smoothed('3smo') temporal and spatial distribution of the given variable. The variable can be:

1. SW: saturation of wetting phase

2. SNdis: saturation of disconnected non-wetting phase
3. SNcon: saturation of connected non-wetting phase
4. PW: pressure of wetting phase
5. PNdis: pressure of disconnected non-wetting phase
6. PNcon: pressure of connected non-wetting phase

plotfreq. Can be used to plot frequency distributions of disconnected region volume, elongatedness, number of pore bodies, specific interfacial area and the pore size distribution.

plotscatter. Can be used to make a scatterplot of all pore bodies containing disconnected non-wetting phase. On the y-axis, the saturation of wetting phase in the pore body is given. On the x-axis, the pore body radius is given.

SNdomSWdom . The scenario has to be specified in the script. Plots disconnected non-wetting phase saturation in the domain vs wetting phase saturation in domain.

References

[1] J. Bear. *Dynamics of fluids in porous media*. Dover publications, 1988.

[2] M.J. Blunt and H. Scher. Pore-level modeling of wetting. *Physical Review E*, 52(6):6387–6403, 1995.

[3] I. Chatzis, N. Morrow, and H. Lim. Magnitude and detailed structure of residual oil saturation. *Old SPE Journal*, 23(2):311–326, 1983.

[4] G.N. Constantinides and A.C. Payatakes. Effects of precursor wetting films in immiscible displacement through porous media. *Transport in porous media*, 38(3):291–317, 2000.

[5] H. Darcy. *Les fontaines publiques de la ville de Dijon*. Dalmont, Paris, 1856.

[6] M.M. Dias and A.C. Payatakes. Network models for two-phase flow in porous media part 1. immiscible microdisplacement of non-wetting fluids. *Journal of Fluid Mechanics*, 164(1):305–336, 1986.

[7] M.M. Dias and A.C. Payatakes. Network models for two-phase flow in porous media, part 2. motion of oil ganglia. *J. Fluid Mech*, 164:337–358, 1986.

[8] D.A. DiCarlo. Quantitative network model predictions of saturation behind infiltration fronts and comparison with experiments. *Water resources research*, 42(7):7408, 2006.

[9] S.M. Hassanizadeh and W.G. Gray. Mechanics and thermodynamics of multiphase flow in porous media including interphase boundaries. *Advances in water resources*, 13(4):169–186, 1990.

[10] S.M. Hassanizadeh and W.G. Gray. Thermodynamic basis of capillary pressure in porous media. *Water Resources Research*, 29(10):3389–3405, 1993.

[11] R.G. Hughes and M.J. Blunt. Pore scale modeling of rate effects in imbibition. *Transport in Porous Media*, 40(3):295–322, 2000.

[12] G.R. Jerauld and S.J. Salter. The effect of pore-structure on hysteresis in relative permeability and capillary pressure: pore-level modeling. *Transport in Porous Media*, 5(2):103–151, 1990.

[13] V. Joekar-Niasar. The immiscibles: Capillarity effects in porous media - pore-network modelling (2. ed.). *Ph.D. thesis, Utrecht University*, 2010.

[14] J. Koplik and T.J. Lasseter. Two-phase flow in random network models of porous media. *Old SPE Journal*, 25(1):89–100, 1985.

[15] K. Mogensen and E.H. Stenby. A dynamic two-phase pore-scale model of imbibition. *Transport in Porous Media*, 32(3):299–327, 1998.

[16] A.C. Payatakes. Dynamics of oil ganglia during immiscible displacement in water-wet porous media. *Annual Review of Fluid Mechanics*, 14(1):365–393, 1982.

[17] J.J. Pickell, B.F. Swanson, and W.B. Hickman. Application of air-mercury and oil-air capillary pressure data in the study of pore structure and fluid distribution. *Old SPE Journal*, 6(1):55–61, 1966.

[18] J.G. Roof. Snap-off of oil droplets in water-wet pores. *Old SPE Journal*, 10(1):85–90, 1970.

[19] M. Tuller and D. Or. Hydraulic conductivity of variably saturated porous media: Film and corner flow in angular pore space. *Water resources research*, 37(5):1257–1276, 2001.

[20] O. Vizika, D.G. Avraam, and A.C. Payatakes. On the role of the viscosity ratio during low-capillary-number forced imbibition in porous media. *Journal of colloid and interface science*, 165(2):386–401, 1994.

[21] N.C. Wardlaw and J.P. Cassan. Oil recovery efficiency and the rock-pore properties of some sandstone reservoirs. *Bulletin of Canadian Petroleum Geology*, 27(2):117–138, 1979.

[22] Wikipedia. http://en.wikipedia.org/wiki/elongatedness, http://en.wikipedia.org/wiki/file:elongatedness.png. 2012.